Structural Study of Acidic Metallocavitands and Characterization of their Interactions with Lewis Bases

*Christian N. Garon,[1] Serge Gorelsky,[2] Olivier Sigouin,[1] Tom K. Woo,[2] and Frédéric-Georges Fontaine[1]**

[1] Département de Chimie, Université Laval, 1045 Avenue de la Médecine, Québec (Québec), Canada, G1V 0A6

[2] Centre for Catalysis Research and Innovation, Department of Chemistry, University of Ottawa, Ottawa (Ontario), Canada, K1N 6N5

frederic.fontaine@chm.ulaval.ca

This is the peer reviewed version of the following article: [Structural Study of Acidic Metallocavitands and Characterization of their Interactions with Lewis Bases,* Inorganic Chemistry, Vol. 48, No. 4, 2009, 1699-1710*], which has been published in final form at [10.1021/ic802233e].

Table of Contents Graphic

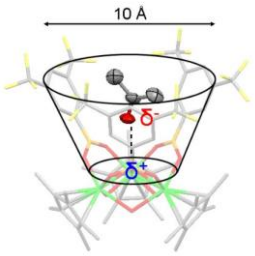

Synopsis

Tantalum boronate metallocavitands reported in this paper can easily be made from various boronic acids and tantalum precursors that are commercially available. These macromolecules adopt a conic structure with an opening of 10 Å and interact specifically with Lewis bases by hydrogen bonding via an μ^3-hydroxide at the bottom center of the cavity and by electrostatic interactions.

Abstract

We report the synthesis and characterization of tantalum-boronate trimetallic clusters of the general formula {[Cp*Ta]$_3$(μ^2-RB(O)$_2$)$_3$(μ^2-OH)(μ^2-O)$_2$(μ^3-OH)} (R= *i*-Bu (**Ta$_3$-*i*Bu**), C_6H_5 (**Ta$_3$-Ph**), 2,5-$(CH_3)_2(C_6H_3)$ (**Ta$_3$-2,5Me**), 3,5-$(CH_3)_2(C_6H_3)$ (**Ta$_3$-3,5Me**), and 3,5-$(CF_3)_2(C_6H_3)$ (**Ta$_3$-3,5CF$_3$**)). Three of these complexes feature a Lewis acid type cavity allowing for substrate binding in both the solid and liquid state using a unique electrostatic interaction and a hydrogen bond. We also report the synthesis of {[Cp*Ta]$_2$(μ^2-MesB(O)$_2$)$_2$[MesB(OH)(O)]$_2$(μ^2-OH)$_2$} (Mes= 2,4,6-$(CH_3)_3C_6H_2$ (**Ta$_2$-Mes**)). All complexes have been characterized by NMR and X-ray diffraction studies, and the steric and electronic effects on the boronate ligands have been investigated. The physical properties of the interaction between the tantalum-boronate clusters and THF and acetone have been studied by thermogravimetric analysis, FT-IR, and DFT calculations in order to characterize the molecular interactions in the resulting adducts.

Introduction

Mutidentate ligands have the ability to rigidify the backbone of transition metal complexes, inducing important properties, such as chirality and durability, as well as paving the way for new supramolecular architectures. The carboxylate moiety has been used abundantly as an organic framework for the synthesis of multimetallic complexes for catalytic purposes[1] or for the creation of metal-organic frameworks.[2] While there are numerous carboxylate complexes, the scarcity of their boron analogues, the alkylboronates, is remarkable. Some alkylboronate complexes have been reported in the literature related to the Suzuki-Miyaura coupling reactions,[3] but early metal analogues are rare. With the exception of the metals of the platinum group,[4,5,6] only Zr,[7] Mn,[8] and Cu[9] boronate complexes were reported. One of the problems with the synthesis of boronate complexes is the weak B-C bond which is susceptible to oxidative coupling; it explains why the platinum group boronate complexes are only transient species. However, with early transition metals, a strong M-O bond stabilizes the ligand coordination to oxophilic transition metals while the high-oxidation state of the metal centers reduces the possibility of B-C bond cleavage, therefore making possible the use of boronate ligands as component of metal-organic supramolecular complexes.

Cavitands are a category of supramolecular assemblies having a bowl-shape structure able to host smaller molecules. The importance of cavitands, such as calixarenes, cucurbiturils, and cyclodextrins in supramolecular chemistry has been put forward in several review articles.[10] They show unique abilities to incorporate guest molecules and to serve as nanovessels for catalysis,[11] for drug delivery,[12] or for molecular recognition.[13] It is also possible to functionalize these macromolecules in order to increase their selectivity for some substrates or to incorporate molecular fragments to suit one's needs;[14] however, the functionalization can prove challenging and generally involves tedious and low yielding multistep syntheses. It is also possible to incorporate a metallic center within or in the periphery of the cavitand to form metallocavitands that serve as mimics to metalloenzymes.[15] However, the strategy involves also multi-step syntheses of organic frameworks. We recently reported the facile one-step synthesis of a new metallocavitand interacting strongly with Lewis bases, {[Cp*Ta]$_3$(μ^2-PhB(O)$_2$)$_3$(μ^2-

$O)_2(\mu^2\text{-OH})(\mu^3\text{-OH})\}$ (**Ta_3-Ph**), from Cp^*TaMe_4 and phenylboronic acid.[16] This new species exhibits interesting features, including a conic cavity somewhat similar to calix[4]arenes, with a pseudo-C_3 symmetry. Even more unique is the presence of four acidic sites at the bottom of the cavity that can, in principle, interact with Lewis bases such as ketones. Since there is a large array of boronic acids commercially available, the possibilities of functionalizing the cavitands' upper-rim are numerous, opening the way to the easy synthesis of supramolecules to use as sensors or catalysts. These metallocavitands can possibly be used for three different functions: 1) as Lewis acids for acid-base recognition and bond activation, 2) as cavitands for size-shape selectivity, and 3) as chemical sensor by having the appropriate functionalized boronate moiety (Figure 1).

Insert Figure 1

In this work, we expand on our previous report by describing the synthesis and characterization of several new Ta(V) boronate clusters, demonstrating the generality of the concept. We will look in more depth at the steric and electronic levels of freedom that are available to form these metallocavitands. An analysis of the physical properties of the interaction between the tantalum clusters and acetone and THF will be described, therefore putting forward the parameters for the construction of more complex assemblies with this supramolecular architecture and explaining the nature of the interaction with Lewis bases.

Results

Synthesis and Crystallographic Studies

We reported that the addition of two equiv. of $RB(OH)_2$ (R = Ph or *i*Bu) to a solution of Cp^*TaMe_4 in presence of one equiv. of water yielded complexes **Ta_3-Ph** and **Ta_3-*i*Bu**, respectively.[16] While both complexes exhibit a typical Ta_3O_4 core observed in various occasions,[17] only the aryl substituted complex is a metallocavitand, since folding of one alkyl chain in **Ta_3-*i*Bu** fills the void made by the

boronate coordination. In order to evaluate the level of freedom available with the steric bulk of substituents on the arylboronic acid, we carried out the synthesis of analogues using boronic acids displaying an increasing amount of steric bulk at the *ortho* and *meta* positions since the *para* position should be easy to modulate without affecting the structure of the cavity. 2,5-dimethylphenylboronic acid and mesitylboronic acid were used to evaluate the effect of a gradual increase in bulk at the carbons situated in *ortho* to the boronate moiety, and 3,5-dimethylphenylboronic acid was used to assess the effects of bulkier substituents at positions far from the boron center. In addition, to study the possible electronic effects in the formation of the cages, electron withdrawing substituents on the aryl fragment of the boronate ligand were used. The reaction was carried out with 3,5-bis(trifluoromethyl)benzeneboronic acid and pentafluorobenzeneboronic acid.

The reaction scheme and the yields for the synthesis of $\{[Cp^*Ta]_3(\mu^2\text{-}2,5\text{-}(CH_3)_2(C_6H_3)B(O)_2)_3(\mu^2\text{-}OH)_2(\mu^2\text{-}O)(\mu^3\text{-}O)\}$ (**Ta$_3$-2,5Me**), $\{[Cp^*Ta]_3(\mu^2\text{-}3,5\text{-}(CH_3)_2(C_6H_3)B(O)_2)_3(\mu^2\text{-}O)_2(\mu^2\text{-}OH)(\mu^3\text{-}OH)\}$ (**Ta$_3$-3,5Me**), and $\{[Cp^*Ta]_3(\mu^2\text{-}3,5\text{-}(CF_3)_2(C_6H_3)B(O)_2)_3(\mu^2\text{-}O)_2(\mu^2\text{-}OH)(\mu^3\text{-}OH)\}$ (**Ta$_3$-3,5CF$_3$**) are shown in Scheme 1 and the solid state structure of the new products and of **Ta$_3$-Ph** obtained by slow evaporation of acetone are illustrated in Figures 2 to 5.

Insert Scheme 1 and Figures 2 to 5

It can be seen from the resolution of the molecular structures of these products that a trimetallic core similar to the one observed with **Ta$_3$-Ph** and **Ta$_3$-*i*Bu** is obtained. In these trimetallic complexes, the tantalum centers are in a pseudo-octahedral environment with the Cp* ligands *trans* to the μ^3-OH while the bridging boronates are *cis* to the μ^2-oxygens. The resulting Ta_3O_4 core possesses a C_2 symmetry caused by the OH groups creating a mirror plane passing through a tantalum center and thus preventing higher symmetry. As a result, one Ta-Ta distance (Ta1-Ta3) and two Ta-O distances (Ta1-O9, Ta3-O9)

are significantly different from the others. The numbering scheme used in this report for the inorganic core can be seen in Figure 6 and a list of relevant interatomic distances are shown in Table 1.

Insert Figure 6 and Table 1

Compounds **Ta_3-3,5Me**, **Ta_3-3,5CF_3**, and **Ta_3-Ph** crystallize with an acetone molecule within the cavity, having weak Van der Waals contacts with one of the boron atoms (3.032 Å for **Ta_3-3,5Me**, 2.928 Å for **Ta_3-3,5CF_3**, and 3.042 Å for **Ta_3-Ph**)[18] and with the μ^3-OH (2.641 Å for **Ta_3-3,5Me**, 2.740 Å for **Ta_3-3,5CF_3**, and 2.646 Å for **Ta_3-Ph**). **Ta_3-3,5Me** and **Ta_3-3,5CF_3** show some level of disorder, with one aryl ring disordered in the former complex and rotational disorder in the trifluoromethyl groups in the latter complex, leading in both cases to two different orientations for the acetone bound inside the cavity. These results indicate that the presence of functional groups in the *meta* position of the aryl ring does not prevent the inclusion of Lewis bases. However, some structural distortion was observed for the aryl groups which are rotated to a certain degree out of the O-B-O plane for **Ta_3-3,5Me** ($13.7°_{av}$) and for **Ta_3-3,5CF_3** ($6.1°_{av}$), whereas the aryl groups are close to co-planarity with the O-B-O plane in **Ta_3-Ph** ($0.9°_{av}$ and $4.4°_{av}$ for THF and acetone containing structures, respectively). In order to limit the repulsion between the *ortho* substituents, the aryl groups in compound **Ta_3-2,5Me** are majorly distorted, as can be seen by the torsion angles of 26.0(4)°, 46.8(3)°, and 54.9(3)°. These torsions result in the cavity of the cluster being completely obstructed and therefore unavailable for Lewis acid-base interactions, since none is observed in the solid state structure. Spacefilling diagrams of the above complexes putting in evidence the cavities are illustrated in Figure 7.

Insert Figure 7

The complex {[Cp*Ta]$_2$(μ^2-MesB(O)$_2$)$_2$[MesB(OH)(O)]$_2$(μ^2-OH)$_2$} (**Ta$_2$-Mes**) was obtained in moderate isolated yield (60%) from the reaction of Cp*TaMe$_4$ with mesitylboronic acid (Scheme 2). X-ray diffraction studies on **Ta$_2$-Mes** showed that a boronic acid bearing substituents on both *ortho* carbons of the aryl fragment displays too much steric bulk to form a trimetallic cluster, as observed in the ORTEP drawing in Figure 8. Instead, a dimer reminiscent of (Cp*)$_2$Zr(η^2-MesBO$_2$)$_2$[7] or [V_2O_3(nicotinate)$_3$][19] is obtained, where two μ^2-boronates bridge two Cp*Ta centers. Interestingly, the steric bulk of the mesityl group did not allow for four bridging boronates so each metal centers features a boronate ligand coordinated in an η^1 fashion and a bridging hydroxo group. The mesityl groups of both the η^1 and η^2 boronate moieties are suffering major rotations out of the O-B-O plane. Torsion angles of 62.9(8)° (η^1), 75.0(8)° (η^1), 50.7(8)° (η^2), and 48.1(8)° (η^2) from the O-B-O plane can be observed in the molecule, and this results in the aromatic rings all aligning in the same plane within the molecule (Figure 9). The rotations out of the plane for the η^2 ligands of **Ta$_2$-Mes** are slightly less than those observed for (Cp*)$_2$Zr(η^2-MesBO$_2$)$_2$ (66.8°).[7] Effectively, this creates π-stacking in the crystal lattice with the interplane distances of around 3.5 Å, where solvent molecules provide support in-between adjacent complexes, since the lattice of the crystal is destroyed when THF is removed upon exposure to air.

Insert Scheme 2 and Figures 8 and 9

The reaction done with pentafluorobenzeneboronic acid resulted in a mixture of products as evidenced by the many Cp* environments between δ 2.0-2.3 ppm observed in the ^{1}H NMR spectrum of the solid crystalline product in C_6D_6. The ^{19}F NMR spectrum of the reaction mixture revealed the only fluorine-containing species to be C_6F_5H when compared to a commercial sample. Separation of the several inorganic products was unsuccessful, but recrystallization attempts yielded two species that were characterized by X-ray diffraction studies. Although the data collected through these studies was of

mediocre quality and therefore unpublishable, we were able to determine that the two major boron products obtained were derivatives of boric acid, as observed in Figure 10. We are still uncertain and are working to assess whether the loss of the C_6F_5 groups happens before or after the formation of the inorganic core of the trimetallic complex.

Insert Figure 10

Metallocavitands as Lewis base guests

Evidence of the hosting behavior in solution of **Ta_3-Ph** is provided by the shielding of the ^{1}H NMR resonances of the inclusion species, which is mainly a consequence of the anisotropic shielding from the aromatic rings. For example, it was observed that the methyl groups of acetone have a chemical shift of 1.36 ppm in benzene-d_6 when acetone is a guest species, compared to the chemical shift of 1.55 ppm for the free molecule. It is therefore informative to look at the ^{1}H chemical shift of acetone in presence of the tantalum clusters in order to probe supramolecular properties in solution.

^{1}H NMR measurements were conducted for all the complexes synthesized throughout this study (Table 2). Other than **Ta_3-Ph,** the trimetallic clusters that show a distinct cavity in the solid state (**Ta_3-3,5Me** and **Ta_3-3,5CF_3**) were found to interact with one equiv. of acetone in solution, as witnessed by the chemical shift sliding upfield by 0.10 and 0.11 ppm, respectively, from the uncoordinated value (δ 1.55 ppm). Electron withdrawing groups on the arylboronate ligands did not seem to have a clear effect on the coordination of acetone in solution versus a complex bearing electron donating substituents. Indeed the chemical shift values observed for these complexes are equivalent to each other and both are lower in magnitude to the shift which is observed for product **Ta_3-Ph** (0.19 ppm). Conversely, studies conducted with **Ta_3-2,5Me** revealed no chemical shift displacement versus the reference uncoordinated acetone value. This supports the observation in the solid state that no cavity is present in the molecule and the conformation observed in the crystal lattice is maintained in solution as well.

Insert Table 2

It was not possible to determinate equilibrium constants at room temperature by ^{1}H NMR, but upon cooling down a toluene-d_8 solution of **Ta$_3$-Ph** and **Ta$_3$-3,5Me**, the coalescence of the acetone resonance was observed at – 70^{o}C and broad peaks were resolved at – 90^{o}C for free (1.39 ppm) and included acetone (0.74 and 0.98 ppm, for **Ta$_3$-Ph** and **Ta$_3$-3,5Me** respectively). The upfield signal for the bound acetone in **Ta$_3$-Ph** suggest a stronger interaction than in **Ta$_3$-3,5Me**, which is confirmed by an association constant of 1.3±0.5 x 10^3 M^{-1} for **Ta$_3$-Ph** which is about one order of magnitude greater than what is observed for **Ta$_3$-3,5Me** (0.8±0.4 x 10^2 M^{-1}). The low solubility of **Ta$_3$-3,5CF$_3$** in cold toluene prevented the determination of the association constant.

In order to quantify the interaction between acetone and THF with complexes having an open cavity at the solid state, a thermogravimetric analysis coupled to mass spectrometry (TGA-MS) was performed on complexes **Ta$_3$-Ph**, **Ta$_3$-3,5Me**, **Ta$_3$-3,5CF$_3$**, and on **Ta$_3$-2,5Me** which does not possess a cavity. A ground, solvent-free sample of the complex was triturated with acetone or THF. The excess solvent was allowed to evaporate for ten minutes on the bench-top and under a continuous flow of air on the scale until the mass of the solid was stabilized.

Any adsorbed solvent molecules on the powder particles of **Ta$_3$-Ph** are instantly lost in the first minutes of the experiment when the mass stabilizes. Upon reaching 46.5°C, a gradual mass reduction process is observed, peaking at 89.0°C and finishing at 126°C for acetone, and peaking at 110°C and finishing at 138°C for THF (Figures 11 and 12, run A). The mass losses observed during these processes total 4.7% (4.2% calculated) for acetone and 8.1% (4.8% calculated) for THF, which are the mass losses expected for one and two molecules of solvent, respectively. These results show that acetone, which has a boiling point of 56°C, is strongly imprisoned in the cavity of **Ta$_3$-Ph** for its optimal evaporation temperature is 89.0°C, which is 33°C more than its boiling point. The same can be said with THF, which has a boiling point of 66°C and leaves the complex optimally at 102°C, 36°C above its boiling point. **Ta$_3$-3,5Me**, with its electron donating methyl groups in *meta* position, could not retain acetone in

the solid state (Figure 11, run B). Indeed, all acetone interacting with the complex is lost during the initialization time since no mass loss is observed until the complex starts to decompose at 150°C. This is an interesting result since the complex demonstrates hosting capacities in solution. However, **Ta_3-3,5Me** can retain THF in the solid state, as a mass loss of 4.9% (calculated and observed) corresponding to one equivalent of THF exiting the cage occurs optimally at 87°C (Figure 12, run B). Isostructural complex **Ta_3-3,5CF_3**, with its electron withdrawing trifluoromethyl groups in *meta* position, lost 2.9% of its total mass during the experiment with acetone (3.2% expected) and had its mass reduction process peak at 96.0°C (Figure 11, run C). This is 7°C above the value observed for **Ta_3-Ph** for a total of 40°C above the boiling point of acetone. Interestingly, experiments conducted with THF as the guest molecule reached a total mass loss of 4.0% (calculated and observed) and had the mass reduction peak at 85°C, which is significantly lower than the result observed with **Ta_3-Ph** and similar to the result obtained with **Ta_3-3,5Me** (Figure 12, run C). Such difference might be the consequence of the larger volume of THF compared to acetone and of a smaller cavity caused by the trifluoromethyl groups.

Insert Figure 11 and Figure 12

Increasing the Lewis acidity at the boron center seems to improve the solvent trapping potential of the cages when steric factors are kept to a minimum. The tests done with the metallocavitands substituted in both *meta* positions of the aryl substituents revealed a certain level of selectivity is attainable by modifying the shape of the opening since **Ta_3-3,5Me** can host THF effectively whereas acetone is easily lost. When the trimetallic species doesn't feature an opening, such as with **Ta_3-2,5Me**, TGA results show no loss of mass until decomposition of the complex, and the same is observed for test runs with silica and carbon exposed to acetone.

We have also attempted to quantify the binding between acetone and the cavitand complexes with DFT calculations at the B3LYP/Lanl2DZ level of theory (Table 3). Geometry optimizations have been performed on **Ta_3-3,5Me**, **Ta_3-Ph**, and **Ta_3-3,5CF_3** (untruncated) with and without acetone bound.

From this, the binding energies, ΔE_b, were calculated to be -13.4, -13.8 and -15.9 kcal mol^{-1} for **Ta$_3$-3,5Me**, **Ta$_3$-Ph**, and **Ta$_3$-3,5CF$_3$**, respectively. This trend agrees with the TGA results in that the peak evaporation temperature was found to be higher for **Ta$_3$-3,5CF$_3$** than for **Ta$_3$-Ph**, while **Ta$_3$-3,5Me** was found not to bind acetone in the solid state. It should be noted that due to the large size of the complexes, it was not feasible to perform harmonic frequency analysis on the full systems, so the binding energies reported do not include zero-point vibrational or free energy corrections. However, we have performed the frequency analysis on a model system {[CpTa]$_3$((C$_6$H$_5$)B(O)$_2$)$_3$(μ^2-OH)$_2$(μ^2-O)(μ^3-O)} in which the Cp* ligands of **Ta$_3$-Ph** are replaced with Cp groups. Binding of acetone to this cluster in the gas phase has a ΔS_b of – 41 cal.mol^{-1}.K^{-1} and a ΔG_b of – 1.6 kcal mol^{-1} at 298K. Since acetone dissociation from the complex should occur when ΔG_b becomes positive, the calculated enthalpy and entropy of the reaction are in good agreement with the temperature of acetone desorption observed by TGA.

We have also examined the binding energy of **Ta$_3$-Ph** with THF, and found it to be -14.8 kcal mol^{-1}, which is 1.0 kcal mol^{-1} stronger than that calculated for acetone. This also agrees with the TGA results which give a peak evaporation temperature of 89°C for acetone and 102°C for THF. On the other hand, the binding energy of THF with **Ta$_3$-Ph** (ΔE_b = -14.8 kcal mol^{-1}) is less than that of acetone with **Ta$_3$-3,5CF$_3$** (-15.9 kcal mol^{-1}), whereas the peak TGA evaporation temperatures suggest it should be higher.

Insert Table 3

Nature of the interaction between the metallocavitand and the Lewis base

The FTIR spectra at the solid state of compounds **Ta$_3$-Ph**, **Ta$_3$-3,5Me,** and **Ta$_3$-3,5CF$_3$** have one sharp peak around 3645 cm^{-1} (3644 cm^{-1} for **Ta$_3$-Ph**, 3645 cm^{-1} for **Ta$_3$-3,5Me**, and 3650 cm^{-1} for **Ta$_3$-3,5CF$_3$**) that can be attributed to the υ_{O-H} stretching frequency. Upon addition of acetone, the sharp signal is lost and one very broad signal centered around 3200 cm^{-1} with a half-width close to 200 cm^{-1} is

observed. However, the broadness of the last signal and the overlap with the C-H stretching frequencies between 3100 and 2700 cm^{-1} prevents a more detailed analysis.

The carbonyl stretching frequency of acetone was monitored as well, once inserted into the cavity. With **Ta_3-Ph**, the carbonyl band shifts to 1708 cm^{-1} and a shoulder appears at 1717 cm^{-1}, relative to the carbonyl band at the gas phase which is expected to be at 1740 cm^{-1}.[20] Complexes **Ta_3-3,5CF_3** and **Ta_3-3,5Me** display similar carbonyl absorption spectrum (Table 4). In order to gain further insight on the nature of the interaction and of the two different stretching frequencies observed for the C=O, computational studies were performed on this system. Since the full systems are too large to perform frequency calculations, a truncated model system $\{[CpTa]_3((C_6H_5)B(O)_2)_3(\mu^2\text{-}OH)_2(\mu^2\text{-}O)(\mu^3\text{-}O)\}$ in which the Cp* ligands of **Ta_3-Ph** are replaced with Cp groups was utilized. The carbonyl stretching frequency was calculated to be 1676 cm^{-1}, which is significantly lower than the experimental value of 1708 cm^{-1}. However, using this somewhat modest basis set, the same band in free acetone is calculated to be 1699 cm^{-1} which is also significantly lower than the experimental value of 1740 cm^{-1}. Thus, the shift in the frequency $\Delta\nu_{CO}$ is calculated to be -23 cm^{-1} which is in reasonable agreement with the shift of -32 cm^{-1} observed experimentally.

Insert Table 4

A distinct shoulder in the carbonyl stretching frequencies suggests that the acetone is bound to the cavitand in at least two distinct configurations. However, all attempts to locate a 2nd distinct binding mode of acetone in our calculated model system or any of the full systems, always led back to the most stable binding geometry. In this way, we found that the cavities of these complexes somewhat more restrictive than expected. To explain the observed shoulder, we considered the more subtle possibility that the acetone is binding to the cavity in the same way, but differently with respect to the bridging μ-OH group of the complex. This is depicted in Figure 13, where the dotted line represents the plane of the bound acetone molecule and the hydrogen atom of the bridging μ-OH group we are discussing is shown

in green. The more symmetric isomer shown in Figure 13a is 0.2 kcal mol^{-1} more stable than the asymmetric isomer shown in Figure 13b. Such a difference in energy is small enough for the two isomers to be present via the Boltzmann population at ambient temperature. Moreover, the calculated red-shift in the carbonyl stretching mode is smaller ($\Delta\nu_{CO}$ = 20 vs. 23 cm^{-1}) for the less stable isomer, that would be corresponding to the shoulder.

Insert Figure 13

The nature of the bonding between the Lewis base and the Ta cavitand is important to understand if one wants to optimize the interaction. Both the acetone and THF interact with the Ta cavitand through a hydrogen bond with the μ^3-OH moiety in the center of the cavity (the ORTEP structures in Figures 2-5 do not show the hydrogen atoms). Without the positions of the hydrogen atoms from the X-ray data, the length of the C=O bond in acetone can be used as a diagnostic parameter to estimate the strength of the hydrogen bond. The crystal structures (as well as the computed structures) reveal that the C=O bond length of acetone only increases by less than 5% relative to the free acetone (Table 1). According to a study done by Novak on the correlation of spectroscopic and crystallographic data, such parameters correspond to a hydrogen bond that is somewhere between weak and intermediate.[21] This suggests that the hydrogen bond alone does not account for the calculated binding energies that were in the range of -13 to -15 kcal mol^{-1}.

We have quantified the amount of orbital interaction and charge transfer between cavitand complexes and the acetone. The Mayer bond order[22] between the O atom of acetone and the H atom of the μ^3-OH moiety for the model complex was found to be only 0.17, which is too small to account for the binding energies calculated. It might be thought that the acetone may be interacting with the B atoms that project into the mouth of the cavity as depicted in Figures 2-5. However, the B-O distances are fairly long, at >3 Å and the calculated Mayer bond orders of 0.01-0.04 suggest there is negligible interaction.

This is also corroborated by the absence of shift upon addition of acetone by $^{11}B\{^{1}H\}$ NMR spectroscopy.

We have also quantified the amount of charge transfer that occurs upon association of the Lewis acid substrate and the Ta cavitands. Analysis of fragment molecular orbital populations of the acetone-Ta_3 model complex, indicates there is a small charge transfer of ~0.14 e^- from acetone to the Ta_3 complex upon the adduct formation. Among all occupied orbitals of acetone, HOMO-3 (55% CO character) makes the largest contribution (0.07 electrons) toward the charge transfer to the Ta_3 cluster. This further suggests that the charge transfer occurs primarily through the O-H hydrogen bond.

Without significant orbital overlap and charge transfer, the attractive interaction between the Lewis base and the Ta cavitands must be dominated by electrostatic interactions. This suggests that the cavitand possesses a favorable electrostatic 'pocket' for the Lewis base. To estimate the electrostatic interaction energy, we have calculated the Natural Population Analysis charges on the free substrate and substrate free Ta complex in the geometry they are in when they form the adduct. We then evaluated the Coulomb interaction energy using these point charges in the geometry of the adduct. The electrostatic interaction energies calculated in this way, ΔE_{ES}, are given in Table 3 for various cavitand/substrate pairs. They range from -17.4 to -22.3 kcal mol^{-1} which compares well with the calculated binding energies that range from -13.4 to -15.9 kcal mol^{-1}. The electrostatic interaction energies are expected to be higher, to offset the unfavorable steric interactions and the energy required to perturb the geometry of the free species to that in the adduct. We can easily correct for the latter, which is commonly known as the preparation energy, by evaluating the energy of the individual adduct forming species in their respective free geometries and comparing it to the energy of the individual species in the geometry they are in the adduct complex. The preparation energies range between 1.3 to 2.3 kcal/mol and the preparation corrected electrostatic interaction energies are given in Table 3 as ΔE_{ES}*. The largest discrepancy between ΔE_{ES}* and the binding energy ΔE_b occurs for the **Ta_3-Ph**-THF complex. For this complex the electrostatic interaction energy is the strongest, but the binding energy is in the middle of the pack. This suggests that the hydrogen bonding interaction between the μ^3-OH group and THF is

weaker than with acetone and that the steric interactions upon adduct formation are stronger. The weaker hydrogen bond with the THF adduct is supported by the slightly smaller O-H bond order of 0.15 for the THF adduct versus 0.17 for the acetone adduct.

To investigate what structural features of cavitand complexes are important in the attractive interaction we have analyzed the NPA charges.[23] The acetone and THF molecules bind with their oxygen atoms directed into the cavity. This suggests that a cavity with a positive electrostatic potential exists to interact favorably with the electronegative end of the substrate. Certainly, the positive charge of the μ^3-OH hydrogen atom that forms the hydrogen bond with the substrate contributes. However, the strength of this hydrogen bond does not account for all of the binding energy, as already established. The B atoms near the bottom of the cavity have large positive charges. For example, the NPA charges on B in **Ta_3-Ph**, are calculated to be approximately +1.2 e (It is notable that the ESP charges on the boron atoms from a CHELPG calculation are also high, ~+0.9e). To see if the charges on the boron atoms have a strong influence on the binding energy, we set their charges to be zero and recalculated the electrostatic binding energy. With the charges set to zero, the electrostatic energy became highly repulsive with ΔE_{ES} = +33.2 kcal mol^{-1}. These calculations strongly suggest that the boron atoms at the mouth of the cavity play a critical role in the binding of Lewis bases. Moreover, it suggests that functionalizing the boron to make it more electropositive will strengthen the substrate binding. To test this, we have calculated the binding energy for Ta_3-F where the Ph group in Ta_3-Ph is replaced by F and found the overall finding energy to be very strong at -17.6 kcal mol^{-1}.

Discussion

There is a large number of cavitands reported in the literature for various host-guest purposes, but most species rely on similar frameworks having C_4 (calix[4]arene, resorcin[4]arene), C_5 (cucurbit[5]uril), C_6 (α-cyclodextrin, cucurbit[6]uril), or higher symmetry (β- and γ-cyclodextrin). The pseudo C_3 symmetry featured in this work is relatively unique and opens new opportunities that are not

easily accessible to other structures, such as chirality, which would be induced by having three different boronate moieties.[24] The association constant measured for acetone and **Ta_3-Ph** at – 90°C (1.3±0.5 x 10^3 M^{-1}) is comparable to many host-guest systems with small molecules, but is several orders of magnitude lower than the strongest binding constants observed for Lewis bases in cavitands (10^5 to 10^8 M^{-1}).[11-13;25] However, it should be noted that THF and acetone are not very strong bases, especially compared to the best systems with DABCO and quinuclidine,[25] and the system we are presenting is intrinsically neutral and no anion-π interaction is present,[15b] which is usually the predominant force in strong interactions within cavitands. Also, the opening of the cavity observed in **Ta_3-Ph** is quite large and the possibility of Van der Waals contacts between the walls of the host and the confined guest, as can be observed with curcubiturils, is limited. Indeed, the metallocavitands can be described as having a conic structure with an approximate diameter of the upper rim of 10 Å, which is relatively similar in size to calix[4]arenes (~8 Å).[26] However, the system we are presenting is one of the simplest: each wall of the cavity is composed of a phenylboronate. We demonstrated that it was possible to functionalize the cavitand by having additional moieties in *meta* position of the arylboronate; the functionalization of the *para* position should therefore be trivial. The modulation of the size of the cavity and the design of architectures with functional groups on the upper-rim would be possible in one synthetic step from one of the many boronic acids commercially available. This fact alone makes this new family of clusters an interesting target for the design of novel supramolecules.

The formation of acid-base pairs in cavitands is not something new; a recent report by Rebek Jr. on deep cavitand having acid functionalities show that the barrier of tumbling of amines within an acid-containing cavitand is raised by 6.5 kcal mol^{-1}.[25] In our system, the positive electrostatic "pocket" at the bottom of the cavity, caused by the presence of the boron atoms, and the hydrogen bond with the μ^3-OH favor the inclusion of Lewis bases with binding energies between –13 and –16 kcal mol^{-1} for acetone and THF. Although there is no bond formed between the boron and the oxygen atom of the guests, the weak Van der Waals contact with boron is significant enough to orientate the acetone and the THF within the cavity. Indeed, in all solid-state structures and in the computational models, only one

orientation is observed for guests, where both lone pairs on oxygen are oriented towards the hydroxide and one boron atom. Nevertheless, the interaction between acetone and **Ta_3-Ph** is stronger than with most examples of multidentate Lewis acids coordinating with ketones.[27] In a previous report, Gabbaï reported that multidentate organomercurials exhibited specific interactions with ketones in solution.[28] However, the interactions at the solid state were weaker and the acetone would evaporate when left for a few minutes on the bench-top and no physical analyses were made.

Concluding Remarks

The complexes described herein are an important addition to the family of boronate ligands coordinated to transition metals for they not only greatly expand the family of reported complexes, they also further our understanding of the assembly and stability of these complexes. Several of the trimetallic species feature an interesting electrophilic cavity, which has been shown to interact with Lewis bases.

Most inclusion complexes having large association constants rely mainly on multiple interactions, such as hydrogen bonding of ionic interactions, or larger pores for guest selectivity. However, the synthetic challenges to obtain these organic hosts are numerous, which can limit the accessibility of the desired molecular architecture. Here, we have described the simplest supramolecular structures that can be made, and still have significant binding energy. While the association constants and the binding energies are comparable to known organic cavitand, it should be kept in mind that the reported complexes bear no special functional groups and a relatively small cavity. It is possible to increase the volume of the cavity or to add functional groups just by modifying the nature of the arylboronic acid, in only one step. We are currently working in adding functional groups on the metallocavitands for the design of sensors and catalysts.

Experimental Section

General Comments. The synthesis of the tantalum clusters were conducted under an atmosphere of nitrogen using standard glovebox techniques. All subsequent manipulations and work-up were done under normal atmosphere. Toluene was purified using a MBraun SPS. Benzene-d_6 and toluene–d_8 were purified by vacuum distillation from Na/K alloy. The elemental analyses were performed at the Laboratoire d'analyse élémentaire de l'Université de Montréal. Cp*TaMe$_4$,[29] **Ta$_3$-Ph**, and **Ta$_3$-iBu**,[16] were prepared according to literature procedures. The boronic acids were purchased from Aldrich, Alfa Aesar, and Frontier Scientific and were used as received. NMR spectra were recorded on a Varian Inova NMR AS400 spectrometer at 400.0 MHz (^{1}H) and 100.0 MHz (^{13}C) or on a Bruker NMR AC-300 at 300 MHz (^{1}H) and 75.5 MHz (^{13}C). The temperatures of the VT NMR experiments were measured using a thermocouple inside the probe which was calibrated with methanol prior to its use.

Synthesis of {[Cp*Ta]$_3$(μ^2-η^2-2,5-(CH$_3$)$_2$C$_6$H$_3$B(O)$_2$)$_3$(μ^2-OH)$_2$ (μ^2-O)(μ^3-O)} (**Ta$_3$-2,5Me**).

A solution of water (9.6 μL, 0.531 mmol) and 2,5-(CH$_3$)$_2$(C$_6$H$_3$)B(OH)$_2$ (159 mg, 1.06 mmol) in THF (5 mL) was added to a solution of Cp*TaMe$_4$ (200 mg, 0.531 mmol) in THF (5 mL) under nitrogen at -78 °C. The resulting yellow solution was stirred for 6 days at room temperature until it turned colorless. The solvent was then removed under reduced pressure. The resulting white precipitate was washed once with acetone (2 mL) in normal atmosphere. The white powder was dried for 5 hours under vacuum at 90°C for the ^{1}H NMR experiments or recrystallized from acetone. Isolated yield: 143 mg, 55%. ^{1}H NMR (benzene-d_6): δ 7.76 (s, 3 H), 6.95 (m, 6 H), 2.26 (ov s, 9 H), 2.24 (ov s, 9 H), 2.11 (br, 15 H), 2.03 (br, 30 H). ^{13}C{^{1}H} NMR (benzene-d_6): δ 140.7, 135.5, 132.5, 129.6, 129.3, 122.1, 22.6, 21.3, 11.6. ^{11}B{^{1}H} NMR (benzene-d_6): 30.3. Anal. Calc. for C$_{54}$H$_{74}$B$_3$O$_{10}$Ta$_3$: C, 44.47; H, 5.11. Found: C, 45.42; H, 5.23.

Synthesis of {[Cp*Ta]$_3$(μ^2-η^2-3,5-(CH$_3$)$_2$C$_6$H$_3$B(O)$_2$)$_3$(μ^2-OH)(μ^2-O)$_2$(μ^3-OH)}.acetone (**Ta$_3$-3,5Me**).

A solution of water (9.6 μL, 0.531 mmol) and 3,5-$(CH_3)_2B(OH)_2$ (159 mg, 1.06 mmol) in THF (5 mL) was added to a solution of Cp*$TaMe_4$ (200 mg, 0.531 mmol) in THF (5 mL) under nitrogen at -78°C. The resulting yellow solution was stirred for 6 days at room temperature until it turned colorless. The solvent was then removed under reduced pressure. The resulting yellow precipitate was washed once with acetone (2 mL) in normal atmosphere. The yellow powder was dried for 5 hours under vacuum at 90°C for the ^{1}H NMR experiments or recrystallized from acetone. Isolated yield: 139 mg, 54%. ^{1}H NMR (benzene-*d*$_6$): δ 7.83 (br s, 4 H), 7.68 (s, 2H), 6.86 (s, 2 H), 6.75 (s, 1 H), 2.25 (ov s, 12 H), 2.24 (ov s, 6 H), 2.19 (br s, 30 H), 2.11 (br s, 15 H). ^{13}C{^{1}H} NMR (benzene-*d*$_6$): δ 139.5, 137.7, 136.1, 135.7, 135.4, 133.9, 133.5, 133.1, 131.5, 131.4, 131.2, 130.7, 130.2, 126.4, 122.5, 122.0, 29.9, 21.7, 21.6, 21.4, 21.0, 11.9, 11.6. ^{11}B{^{1}H} NMR (benzene-*d*$_6$): 24.0. Anal. Calc. for $C_{54}H_{74}B_3O_{10}Ta_3$: C, 44.47; H, 5.11 %. Found: C, 44.37; H, 5.28 %.

Synthesis of {[Cp*Ta]$_3$(μ^2-η^2-3,5-$(CF_3)_2C_6H_3B(O)_2$)$_3$(μ^2-OH)$_2$(μ^2-O)(μ^3-O)}.acetone (**Ta$_3$-3,5CF$_3$**). A solution of water (7.2 μL, 0.399 mmol) and 3,5-$(CF_3)_2C_6H_3B(OH)_2$ (210 mg, 0.814 mmol) in THF (5 mL) was added to a solution of Cp*$TaMe_4$ (150 mg, 0.399 mmol) in THF (5 mL) under nitrogen at -78°C. The resulting yellow solution was stirred for 6 days at room temperature until it turned colorless. The solvent was then removed under reduced pressure. The resulting yellow precipitate was washed once with acetone (2 mL) in normal atmosphere. The white powder was dried for 5 hours under vacuum at 90°C for the ^{1}H NMR experiments or recrystallized from acetone. Isolated yield: 146 mg, 75%. ^{1}H NMR (acetone-*d*$_6$): δ 8.31 (s, 4 H), 8.25 (s, 2 H), 7.89 (s, 3 H), 2.30 (ov s, 30 H), 2.27 (ov s, 15 H). ^{13}C{^{1}H} NMR (acetone-*d*$_6$): δ 145.1, 136.6, 131.7, 129.9, 127.2, 125.2, 124.7, 124.5, 124.0, 121.8, 13.1, 12.9. ^{11}B{^{1}H} NMR (acetone-*d*$_6$): 27.6. ^{19}F{^{1}H} NMR (acetone-*d*$_6$) : δ −64.1. Anal. Calc. for $C_{54}H_{56}B_3O_{10}F_{18}Ta_3$: C, 36.39; H, 3.17 %. Found: C, 36.88; H, 3.11 %.

Synthesis of {[Cp*Ta]$_2$(μ^2-η^2-MesB(O)$_2$)$_2$[η^1-MesB(O)(OH)]$_2$(μ^2-OH)$_2$} (**Ta$_2$-Mes**).

A solution of water (9.6 μL, 0.531 mmol) and 2,4,6-$(CH_3)_3(C_6H_2)B(OH)_2$ (175 mg, 1.07 mmol) in THF (5 mL) was added to a solution of Cp*$TaMe_4$ (200 mg, 0.531 mmol) in THF (5 mL) under nitrogen at -78°C. The resulting yellow solution was stirred for 4 days at room temperature until it turned colorless. The solvent was then removed under reduced pressure. The resulting white precipitate was washed once with acetone (2 mL) in normal atmosphere to yield a clean white powder. Isolated yield: 133 mg, 38%. ^{1}H NMR (toluene-*d*$_8$, -40°C): δ 7.00 (s, 2H), 6.86 (s, 2H), 2.71 (s, 6H), 2,49 (s, 6H), 2.31 (d, $^4J_{H\text{-}H}$ = 8.8 Hz, 6H), 1.90 (s, 15H). ^{11}B{^{1}H} NMR (chloroform-*d*): 31.2. Anal. Calc. for $C_{56}H_{78}B_4O_{10}Ta_2$: C, 51.10; H, 5.97 %. Found C, 51.53; H, 6.37 %. The low solubility of Ta_2-Mes prevented from taking a ^{13}C{^{1}H} NMR spectrum.

Reaction of Cp*$TaMe_4$ with $C_6F_5B(OH)_2$.

A solution of water (9.6 μL, 0.531 mmol) and 3,5-$(CF_3)_2C_6H_3B(OH)_2$ (225 mg, 1.07 mmol) in THF (5 mL) was added to a solution of Cp*$TaMe_4$ (200 mg, 0.531 mmol) in THF (5 mL) under nitrogen at -78°C. The resulting dark yellow solution was stirred for 2 days at room temperature until it turned pale yellow. The solvent was then removed under reduced pressure. The resulting yellow precipitate was dissolved in acetone (2 mL) in normal atmosphere and recrystallized into clear colorless crystals. Yield: 138 mg. ^{1}H NMR (benzene-*d*$_6$, ppm): δ 2.0-2.3 (m).

Binding Constant Determination.

The binding constants were determined by ^{1}H NMR. Solutions of the cavitand were prepared at known concentrations in deuterated toluene and roughly one equivalent of acetone was added to the mixture. An initial spectrum was recorded at room temperature with a 30s pulse delay to improve the accuracy of the integrations and the exact concentration of acetone in solution was obtained. A second spectrum was recorded at -90°C with 30s pulse delay and concentrations for the trapped and free acetone

were obtained. The binding constants were then calculated from the equation: [Ta.acetone] / $[Ta]_{free}[acetone]_{free}$. All experiments were duplicated with separate samples.

Crystallographic data.

Crystallographic data are reported in Table 5. Single crystals were coated with Paratone-N oil, mounted using a glass fibre and frozen in the cold nitrogen stream of the goniometer. The data were collected on a Bruker SMART APEX II diffractometer. The data were reduced (SAINT)[30] and corrected for absorption (SADABS).[31] The structure was solved and refined using SHELXS-97 and SHELXL-97.[32] All non-H atoms were refined anisotropically. The hydrogen atoms were placed at idealized positions, but the hydrogen atoms on the hydroxyl ligands are missing since they were not located. Neutral atom scattering factors were taken from the International Tables for X-Ray Crystallography.[33] All calculations and drawings were performed using the SHELXTL package.[34] The final model was checked either for missed symmetry or voids in the crystal structure using the PLATON software.[35] None was found. The crystal structures gave a satisfactory chekcif report.

Insert Table 5

Thermogravimetric analyses.

TG-MS measurements were performed using a Netzsch STA 449C thermogravimetric analyser coupled with a Netzsch Aeolos QMS 403C mass spectrometer. For complexes with acetone binding, the experiments were conducted over a range of 150°C, from 34°C to 184°C. THF experiments were conducted from 35°C to 200°C. The temperature was increased at a rate of 5°C/min.

FTIR

Spectra were recorded using a Nicolet Magna 850 Fourier transform infrared spectrometer (Thermo Scientific, Madison, WI) with a liquid nitrogen cooled narrow-band mercury cadmium telluride (MCT)

detector and a Golden Gate ATR accessory (Specac Ltd., London, UK). In this apparatus, the infrared beam is focused to a diameter of about 500 μm on the diamond crystal with ZnSe lenses (4X magnification). Each spectrum was obtained from 128 scans at a resolution of 4 cm^{-1} using a Happ–Genzel apodization. No further spectral operations were performed on obtained spectra.

Computational Section

Density Functional Theory (DFT) calculations have been performed using *Gaussian 03*[36] program at the B3LYP[37]/LanL2DZ[38] level. Geometry optimizations and electronic structure analysis calculations were completed using the spin-restricted method. Wave function stability calculations[39] were performed to confirm that the calculated wave functions corresponded to the true electronic ground state. Tight SCF convergence criteria (10^{-8} a.u.) were used for all calculations. Harmonic frequency calculations were used to determine the nature of the stationary points, vibrational frequencies and the thermodynamic parameters (at 298 K and 1 atm.) for the cyclopentadienyl (Cp) models of the Ta clusters. The analysis of the electronic structure was performed using *Gaussian 03* calculations at the same level of theory as geometry optimizations. Orbital populations and compositions were calculated using Mulliken population analysis (MPA) using the *AOMix* program.[40] Mayer bond orders[41] were calculated using the *AOMix-L* program. Atomic charges were evaluated by using the natural population analysis (NPA).[42]

The energies of electrostatic interactions were evaluation using the point-charge approximation:

$$E_{ES} = \sum_{a \in Ta} \sum_{b \in X} \frac{q_a^{NPA} q_b^{NPA}}{r_{ab}}$$ (in atomic units).

where q^{NPA} are NPA-derived atomic charges in the two non-interacting fragments, Ta_3 and the substrate, with the geometry of the adduct. r_{ab} are the corresponding interatomic distances in the adduct structure.

Acknowledgment. We are grateful to NSERC (Canada), CFI (Canada), FQRNT (Québec), and Université Laval for financial support. T. K. Woo acknowledge the Canada Research Chairs program. C. N. Garon acknowledges FQRNT for a scholarship. We acknowledge C. Tessier for their help solving the solid state structures. We acknowledge F. Kleitz and L. Marcoux (Université Laval) for their help with TGA and J.-F. Rioux (Université Laval) for their help with FTIR.

Supporting Information Available: ^{1}H NMR and FTIR spectra of selected compounds. This material is available free of charge via the Internet at http://pubs.acs.org. Crystallographic data have been deposited with CCDC (CCDC No. 704431 for **Ta_2-Mes**, CCDC No. 704432 for **Ta_3-2,5Me**, CCDC No. 704433 for **Ta_3-3,5Me.acetone**, CCDC No. 704434 for **Ta_3-Ph.acetone**, and CCDC No. 704435 for **Ta_3-3,5CF_3.acetone**). These data can be obtained upon request from the Cambridge Crystallographic Data Centre, 12 Union Road, Cambridge CB2 1EZ, UK, e-mail: deposit@ccdc.cam.ac.uk, or via the internet at www.ccdc.cam.ac.uk.

References

[1] Davies, H. M. L.; Beckwith, R. E. J. *Chem. Rev.* **2003**, *103*, 2861-2904.

[2] a) Férey, G. *Chem. Soc. Rev.* **2008**, *37*, 191-214 ; b) James, S. L. *Chem. Soc. Rev.* **2003**, *32*, 276-288; c) Eddaoudi, M. ; Moler, D. B. ; Li, H. ; Chen, B. ; Reineke, T. M. ; O'Keeffe, M. ; Yaghi, O. M. *Acc. Chem. Res.* **2001**, *34*, 319-330.

[3] Miyaura, N.; Suzuki, A. *Chem. Rev.* **1995**, *95*, 2457-2483.

[4] a) Ahijado, M.; Braun, T. *Angew. Chem. Int. Ed.* **2008**, *47*, 2954-2958; b) Zhao, P.; Incarvito, C. D.; Hartwig, J. F. *J. Am. Chem. Soc.* **2007**, *129*, 1876-1877.

[5] Crociani, B.; Antonaroli, S.; Marini, A.; Matteoli, U.; Scrivanti, A. *Dalton Trans.* **2006**, 2698-2705.

[6] a) Pantcheva, I.; Osakada, K. *Organometallics* **2006**, *25*, 1735-1741; b) Pantcheva, I.; Nishihara, Y.; Osakada, K. *Organometallics* **2005**, *24*, 3815-3817.

[7] Balkwill, J. E.; Cole, S. C.; Coles, M. P.; Hitchcock, P. B. *Inorg. Chem.* **2002**, *41*, 3548-3552.

[8] a) Marlin, D. S.; Bill, E.; Weyhermüller, T.; Bothe, E.; Wieghardt, K. *J. Am. Chem. Soc.* **2005**, *127*, 6095-6108; b) Duboc-Toia, C.; Hummel, H.; Bill, E.; Barra, A.-L.; Chouteau, G.; Wieghardt, K. *Angew. Chem. Int. Ed.* **2000**, *39*, 2888-2890; c) Bossek, U.; Hummel, H.; Weyhermüller, T.; Wieghardt, K.; Russell, S.; van der Wolf, L.; Kolb, U. *Angew. Chem. Int. Ed.* **1996**, *35*, 1552-1554.

[9] Bardwell, D. A.; Jeffery, J. C.; Ward, M. D. *Polyhedron* **1996**, *15*, 2019-2022.

[10] a) Liu, S.; Gibb, B. C. *Chem. Commun.* **2008**, 3709-3716; b) Biros, S. M.; Rebek Jr., J. *Chem. Soc. Rev.* **2007**, *36*, 93-104; c) Houk, K. N.; Leach, A. G.; Kim, S. P.; Zhang, X. *Angew. Chem. Int. Ed.* **2003**, *42*, 4872-4897.

[11] Few leading references: a) Shenoy, S. R.; Pinacho Crisóstomo, F. R.; Iwasawa, T.; Rebek, J. *J. Am. Chem. Soc.* **2008**, *130*, 5658-5659; b) Zelder, F. H.; Rebek Jr., J. *Chem. Commun.* **2006**, 753-754; c) Gissot, A.; Rebek Jr., J. *J. Am. Chem. Soc.* **2004**, *126*, 7424-7425.

[12] Few leading references: a) Kuykendall, D. W.; Zimmerman, S. C. *Nat. Nanotechnol.* **2007**, *2*, 201-202; b) Memisoglu-Bilensoy, E.; Dogan, A. L.; Hincal, A. A. *J. Pharm. Pharmacol.* **2006**, *58*, 585-589.

[13] Few leading references: a) Schramm. M. P.; Rebek Jr., J. *Chem. Eur. J.* **2006**, *12*, 5924-5933; b) Pinalli, R.; Suman, M.; Dalcanale, E. *Eur. J. Org. Chem.* **2004**, 451-462; c) Arimori, S.; Davidson, M. G.; Fyles, T. M.; Hibbert, T. G.; James, T. D.; Kociok-Köhn, G. I. *Chem. Commun.* **2004**, 1640-1641.

[14] Few leading references: a) Srinivasan, K.; Laughrey, Z. R.; Gibb, B. C. *Eur. J. Org. Chem.* **2008**, 3265-3271; Azov, V. A.; Schlegel, A.; Diederich, F. *Bull. Chem. Soc. Jpn.* **2006**, *79*, 1926-1940; c) Aakeröy, C. B.; Schultheiss, N.; Desper, J. *Org. Lett.* **2006**, *8*, 2607-2610; d) Harvey, P. D. *Coord. Chem. Rev.* **2002**, *233-234*, 289-309.

[15] Few leading references: a) Frischmann, P. D.; MacLachlan, M. J. *Comments Inorg. Chem.* **2008**, *29*, 26-45; b) Lenthall, J. T.; Steed, J. W. *Coord. Chem. Rev.* **2007**, *251*, 1747-1760; c) Jeunesse, C.; Armspach, D.; Matt, D. *Chem. Commun.* **2005**, 5603-5614.

[16] Sigouin, O.; Garon, C. N.; Delaunais, G.; Yin, X.; Woo, T. K.; Fontaine, F.-G. *Angew. Chem. Int. Ed.* **2007**, *46*, 4979-4982.

[17] a) Blaurock, S.; Hey-Hawkins, E. *Eur. J. Inorg. Chem.* **2002**, 2975-2984; b) Jernakoff, P.; De Meric de Bellefon, C.; Geoffroy, G. L.; Rheingold, A. L.; Geib, S. J. *Organometallics* **1987**, *6*, 1362-1364.

[18] Since all acetone molecules are disordered, only the average values without the esds are given in most crystallographic data.

[19] Lin, W.; Ayyappan, P. *Polyhedron* **2003**, *22*, 3037-3042.

[20] Pimentel, G. C.; McClellan, A. L. *The Hydrogen Bond*; W. H. Freeman and Company: San Francisco, CA, 1960; p 139.

[21] Novak, A. Hydrogen Bonding in Solids. Correlation of Spectroscopic and Crystallographic Data. In *Structure & Bonding*; Springer: Berlin, 1974; Vol. 18, pp 177-216.

[22] Mayer, I. *Chemical Physics Letters* **1983**, *97*, 270-274.

[23] Reed, A. E.; Weinstock, R. B.; Weinhold, F. *J. Chem. Phys.* **1985**, *83*, 735-746.

[24] **Ta_3-Ph** is stable in presence of water and of various boronic acids and no boronate exchange as yet been observed, other that the decomposition of the complex obtained from the reaction with $C_6F_5B(OH)_2$ *(vide supra*). However, the step by step post-functionalization of a *para*-X-phenylboronate cluster (X = Br, I) and the resolution of the racemic mixture would be possible.

[25] Purse, B. W.; Butterfield, S. M.; Ballester, P.; Shivanyuk, A.; Rebek Jr., J. *J. Org. Chem.* **2008**, *73*, 6480-6488.

[26] Average value determined by looking at 795 structures of calix[4]arene in Cambridge Crystallographic Database.

[27] a) Wuest, J. D. *Acc. Chem. Res.* **1999**, *32*, 81-89; b) Maruoka, K. *Pure Appl. Chem.* **2002**, *74*, 123-128; c) Simard, M.; Vaugeois, J.; Wuest, J. D. *J. Am. Chem. Soc.* **1993**, *115*, 370-372.

[28] a) Tschinkl, M.; Schier, S.; Riede, J.; Gabbaï, F. P. *Organometallics* **1999**, *18*, 1747-1753. b) Beckwith King, J.; Tsunoda, M.; Gabbaï, F. P. *Organometallics* **2002**, *21*, 4201-4205.

[29] Sanner, R. D.; Carter, S. T.; Bruton Jr., W. J. *J. Organomet. Chem.* **1982**, *240*, 157-162.

[30] *SAINT* Version 7.07a; Bruker AXS Inc.: Madison, WI, 2003.

[31] Sheldrick, G. M. *SADABS* Version 2004/1; Bruker AXS Inc.: Madison, WI, 2004.

[32] Sheldrick, G. M. *SHELXS-97 and SHELXL-97. Programs for the refinement of crystal structures*; University of Gottingen: Germany, 1997.

[33] *International Tables for Crystallography, Vol C.*, Wilson, A. J. C., Ed. Kluwer Academic Publishers: Dordecht, 1992, pp 219-222 and pp. 500-502.

[34] *SHELXTL*. Version 6.12; Bruker AXS: Madison, WI, 2001.

[35] Spek, A. L. *PLATON*, *A Multipurpose Crystallographic Tool*; University of Utrecht: Utrecht, The Netherlands, 2005.

[36] Frisch, M. J.; Trucks, G. W.; Schlegel, H. B.; Scuseria, G. E.; Robb, M. A.; Cheeseman, J. R.; Montgomery, J., J. A. ; Vreven, T.; Kudin, K. N.; Burant, J. C.; Millam, J. M.; Lyengar, S. S.; Tomasi, J.; Barone, V.; Mennucci, B.; Cossi, M.; Scalmani, G.; Rega, N.; Petersson, G. A.; Nakatsuji, H.; Hada, M.; Ehara, M.; Toyota, K.; Fukuda, R.; Hasegawa, J.; Ishida, M.; Nakajima, T.; Honda, Y.; Kitao, O.; Nakai, H.; Klene, M.; Li, X.; Knox, J. E.; Hratchian, H. P.; Cross, J. B.; Adamo, C.; Jaramillo, J.; Gomperts, R.; Stratmann, R. E.; Yazyev, O.; Austin, A. J.; Cammi, R.; Pomelli, C.; Ochterski, J. W.; Ayala, P. Y.; Morokuma, K.; Voth, G. A.; Salvador, P.; Dannenberg, J. J.; Zakrzewski, V. G.; Dapprich, S.; Daniels, A. D.; Strain, M. C.; Farkas, O.; Malick, D. K.; Rabuck, A. D.; Raghavachari, K.; Foresman, J. B.; Ortiz, J. V.; Cui, Q.; Baboul, A. G.; Clifford, S.; Cioslowski, J.; Stefanov, B. B.; Liu, G.; Liashenko, A.; Piskorz, P.; Komaromi, I.; Martin, R. L.; Fox, D. J.; Keith, T.; Al-Laham, M. A.; Peng, C. Y.; Nanayakkara, A.; Challacombe, M.; Gill, P. M. W.; Johnson, B.; Chen, W.; Wong, M. W.; Gonzalez, C.; Pople, J. A.; Gaussian, Inc.: 2003.

[37] a) Becke, A. D. *J. Chem. Phys.* **1993**, *98*, 5648. b) Lee, C.; Yang, W.; Parr, R. G. *Phys. Rev.* **1988**, *B37*, 785.

[38] a) Hay, P. J.; Wadt, W. R. *J. Chem. Phys.* **1985**, *82*, 299-310 (b) Hay, P. J.; Wadt, W. R. *J. Chem. Phys.* **1985**, *82*, 270-283. (c) Wadt, W. R.; Hay, P. J. *J. Chem. Phys.* **1985**, *82*, 284-298.

[39] Bauernschmitt, R.; Ahlrichs, R. *J. Chem. Phys.* **1996**, *104*, 9047-9052.

[40] Gorelsky, S. I.; version 6.36 ed.; University of Ottawa: Ottawa, Canada, 2007.

[41] Mayer, I. *Chemical Physics Letters* **1983**, *97*, 270-274.

[42] Reed, A. E.; Weinstock, R. B.; Weinhold, F. *J. Chem. Phys.* **1985**, *83*, 735-746.

Tables

Table 1. Distances of interest in structurally characterized Ta_3 complexes.

Complexe	dTa1-Ta2 (Å)	dTa2-Ta3 (Å)	dTa1-Ta3 (Å)	dTa1-O9 (Å)	dTa3-O9 (Å)	dC90-O90 (Å)
Ta_3-*i*Bu	3.341	3.340	3.320	2.073	2.068	-
Ta_3-Ph.acetone	3.333	3.333	3.453	2.092	2.092	1.161
Ta_3-Ph.THF	3.346	3.345	3.428	2.092	2.092	-
Ta_3-2,5Me	3.370	3.412	3.214	1.972	1.975	-
Ta_3-3,5Me	3.376	3.408	3.303	1.974	1.963	1.212
Ta_3-3,5CF_3	3.310	3.296	3.503	2.145	2.144	1.225

Table 2. ^1H chemical shift of bound and free acetone in adducts of Ta_3 complexes in a C_6D_6 solution.

Complex	δ (ppm)
free acetone	1.55
Ta_3-Ph	1.36
Ta_3-*i*Bu	1.54
Ta_3-2,5Me	1.53
Ta_3-3,5Me	1.45
Ta_3-3,5CF_3	1.44

Table 3. Calculated binding energies between Ta_3 complexes and substrate.

complex	substrate molecule	ΔE_b[a] (kcal mol^{-1})	ΔE_{ES}[b] (kcal mol^{-1})	ΔE_{ES}*[c] (kcal mol^{-1})
Ta_3-3,5Me	acetone	-13.4	-17.8	-16.1
Ta_3-Ph	acetone	-13.8	-17.4	-15.6
Ta_3-Ph	THF	-14.8	-22.3	-19.7
Ta_3-3,5CF_3	acetone	-15.9	-19.7	-18.4
Ta_3-F	acetone	-17.6	-21.0	-18.7

[a]binding energy calculated at the B3LYP/Lanl2DZ level of theory. [b]electrostatic interaction energy calculated using NPA point charges (see text for more details). c) electrostatic interaction energy, including the preparation energy, or the energy required to distort the adduct forming species from there free geometry to the geometry in the adduct complex.

Table 4. Carbonyl stretching frequencies for acetone with Ta_3 complexes.

Complex	Experimental Carbonyl Band (cm^{-1})		Calculated Carbonyl Band (cm^{-1})
	Major component	Shoulder	
Gaseous acetone	1740	-	1699
Ta_3-Ph	1708	1717	1676[a]
Ta_3-3,5Me	1703	1715	-
Ta_3-3,5CF_3	1706	1713	-

[a]carbonyl stretch frequency calculated on a truncated model of **Ta_3-Ph**, where the Cp* have been replaced by Cp ligands (see text for more details).

Table 5. Crystal data, data collection, and structure refinement for Ta_3 complexes and Ta_2-Mes

	Ta_3-2,5Me	Ta_3-3,5Me	Ta_3-3,5CF_3	Ta_3-Ph.acetone	Ta_2-Mes
formula	$C_{54}H_{72}B_3O_{10}Ta_3$	$C_{54}H_{72}B_3O_{10}Ta_3$, C_3H_6O	$C_{54}H_{54}B_3O_{10}F_{18}Ta_3$, C_3H_6O	$C_{54}H_{74}B_3O_{12}Ta_3$, C_3H_6O	$C_{56}H_{48}B_4O_{10}Ta_2$, $2(C_4H_8O)$
fw	1457.4	1514.47	1838.33	1548.50	1460.53
size (mm)	0.30 x 0.24 x 0.20	0.18 x 0.11 x 0.10	0.3 x 0.2 x 0.2	0.3 x 0.3 x 0.2	0.15 x 0.16 x 0.06
cryst syst	Monoclinic	Triclinic	Triclinic	Monoclinic	Triclinic
space group	P2(1)/n	P-1	P-1	P2(1)/n	P-1
a (Å)	14.2618(5)	12.313(3)	12.554(3)	12.2119(8)	13.6909(19)
b (Å)	20.0522(7)	12.435(3)	12.669(3)	17.2175(11)	16.068(2)
c (Å)	18.4914(6)	20.171(3)	21.659(6)	14.6516(10)	16.587(2)
α (deg)	90	87.105(3)	83.460(3)	90	97.783(2)
β (deg)	90.34(1)	83.411(3)	78.659(3)	111.5270(10)	110.322(2)
γ (deg)	90	74.300(3)	74.210(3)	90	107.834(2)
V ($Å^3$)	5288.1(3)	2952.9(12)	3243.3(14)	2865.7(3)	3135.3(7)
Z	4	2	2	2	2
Wavelength (Å)	0.71073	0.71073	0.71073	0.71073	0.71073
$D_{calc.}$ ($mg.m^{-3}$)	1.831	1.703	1.882	1.727	1.547
F_{000}	2844	1484	1772	1456	1480
Temp (K)	100(2)	200(2)	200(2)	200(2)	100(2)
no. of unique/total reflns	12872 / 64497	13711 / 34427	15322 / 38820	7188/35331	12270 / 33865
R_{int}	0.0266	0.0379	0.0722	0.0243	0.0474
Final R indices [I>2σ(I)]	R1 = 0.0179 wR2 = 0.0466	R1 = 0.0318 wR2 = 0.0629	R1 = 0.0489 wR2 = 0.1214	R1 = 0.0243 wR2 = 0.0579	R1 = 0.0371 wR2 = 0.0836

Schemes

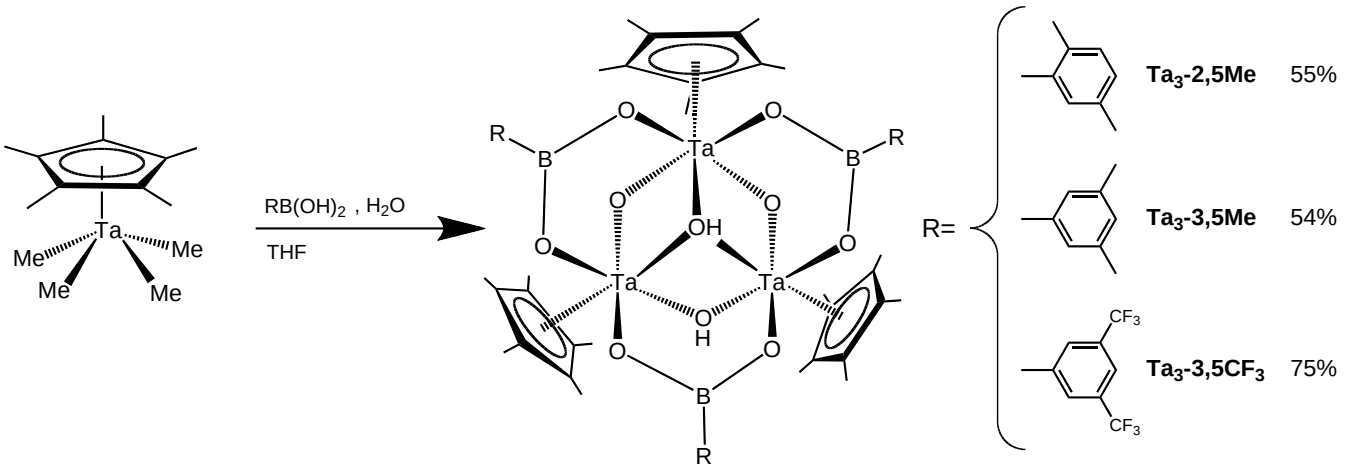

Scheme 1. Synthesis of **Ta_3-2,5Me**, **Ta_3-3,5Me**, and **Ta_3-3,5CF_3**.

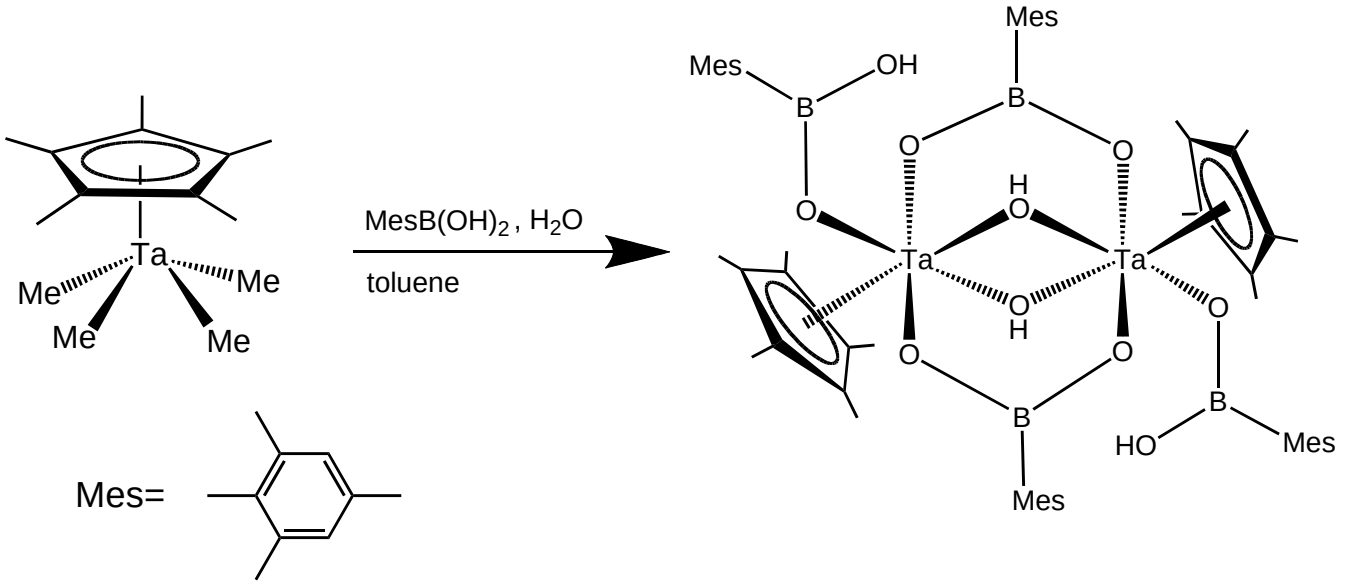

Scheme 2. Synthesis of **Ta_2-Mes**.

Figure Captions

Figure 1. General design of tantalum(V) boronate metallocavitand having: A) a Lewis acid site, B) a cavitand, and C) a chemical sensor.

Figure 2. ORTEP diagram (50% probability) of **Ta_3-2,5Me**. Hydrogen atoms have been omitted for clarity.

Figure 3. ORTEP diagram (50% probability) of **Ta_3-3,5Me.acetone**. Only one model for the disordered aryl group on B3 is shown. Hydrogen atoms have been omitted for clarity.

Figure 4. ORTEP diagram (50% probability) of **Ta_3-3,5CF_3.acetone**. Only one model for the disordered CF_3 is shown. Hydrogen atoms have been omitted for clarity.

Figure 5. ORTEP diagram (50% probability) of **Ta_3-Ph.acetone**. Only one model for the disordered acetone is shown. Hydrogen atoms have been omitted for clarity.

Figure 6. Labelling scheme for the inorganic core of Ta_3 complexes.

Figure 7. Spacefilling of (top to bottom, left to right) **Ta_3-Ph**, **Ta_3-*i*Bu**, **Ta_3-2,5Me**, **Ta_3-3,5Me**, and **Ta_3-3,5CF_3**.

Figure 8. ORTEP diagram (50% probability) of **Ta_2-Mes**. Hydrogen atoms have been omitted for clarity.

Figure 9. Packing diagram of **Ta_2-Mes.THF**.

Figure 10. Major products obtained from the reaction of 2 equiv of $C_6F_5B(OH)_2$ with Cp*$TaMe_4$.

Figure 11. TGA of A) **Ta_3-Ph** (▬), B) **Ta_3-3,5Me** (─), and C) **Ta_3-3,5CF_3** (- - -) with acetone.

Figure 12. TGA of A) **Ta_3-Ph** (▬), B) **Ta_3-3,5Me** (─), and C) **Ta_3-3,5CF_3** (- - -) with THF.

Figure 13. a) Lowest energy isomer and b) higher-energy isomer of the Ta_3-Ph adduct with acetone. The dashed line represents the intersection between the plane of the acetone molecule in the adduct with the plane made by the three Ta atoms. The H atom of the μ^2-OH group is shown in green. The Cp ligands and the Ph groups of the Ta_3 clusters and the Me groups of acetone are not shown for clarity.

Figures

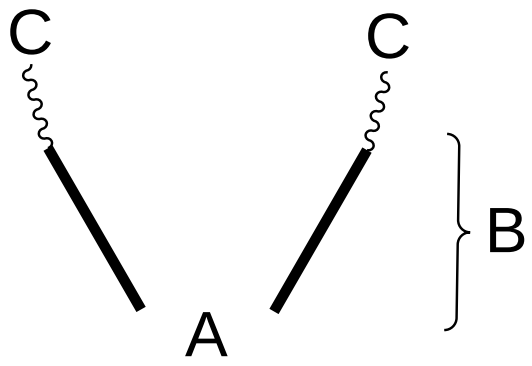

Figure 1.

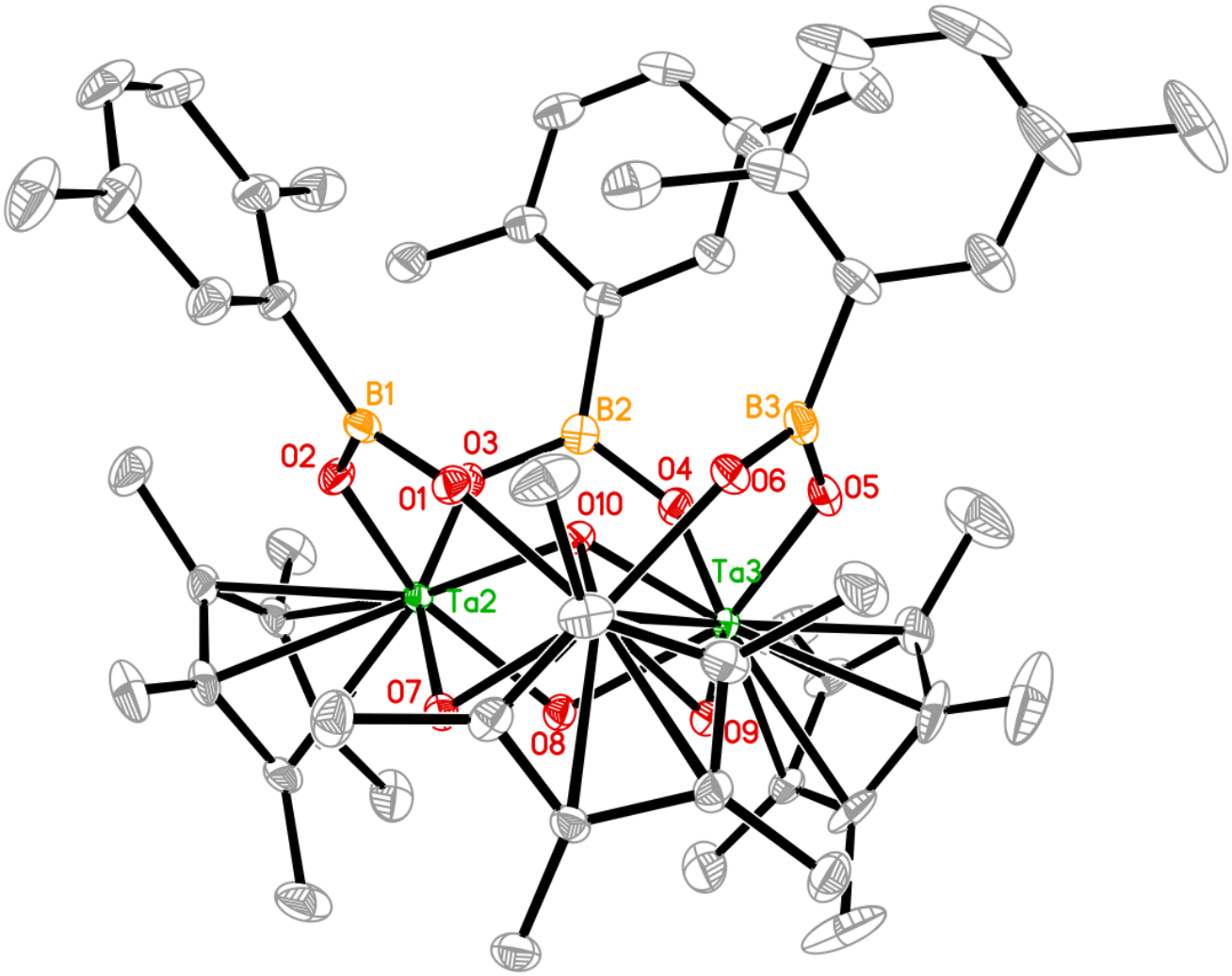

Figure 2.

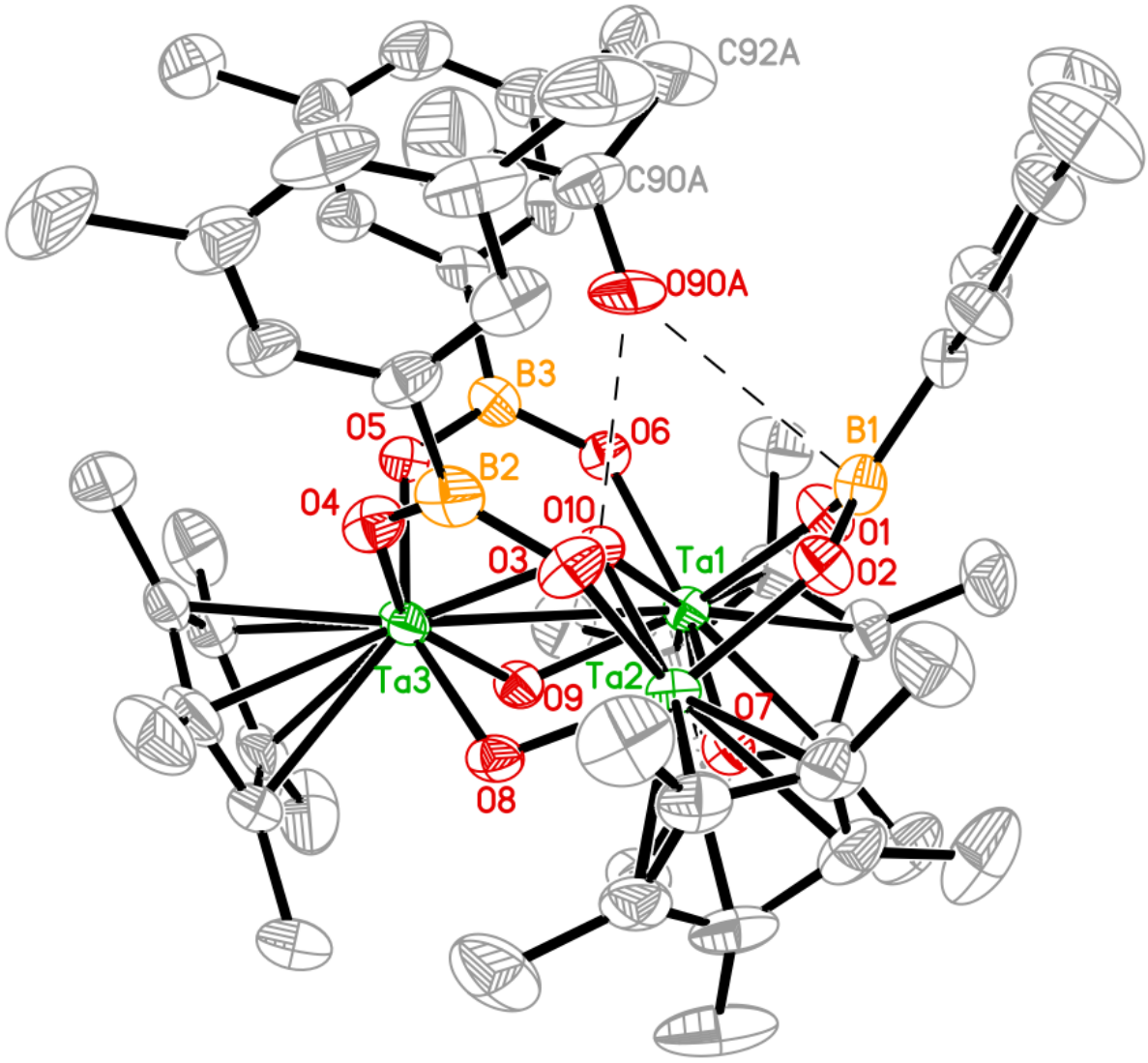

Figure 3.

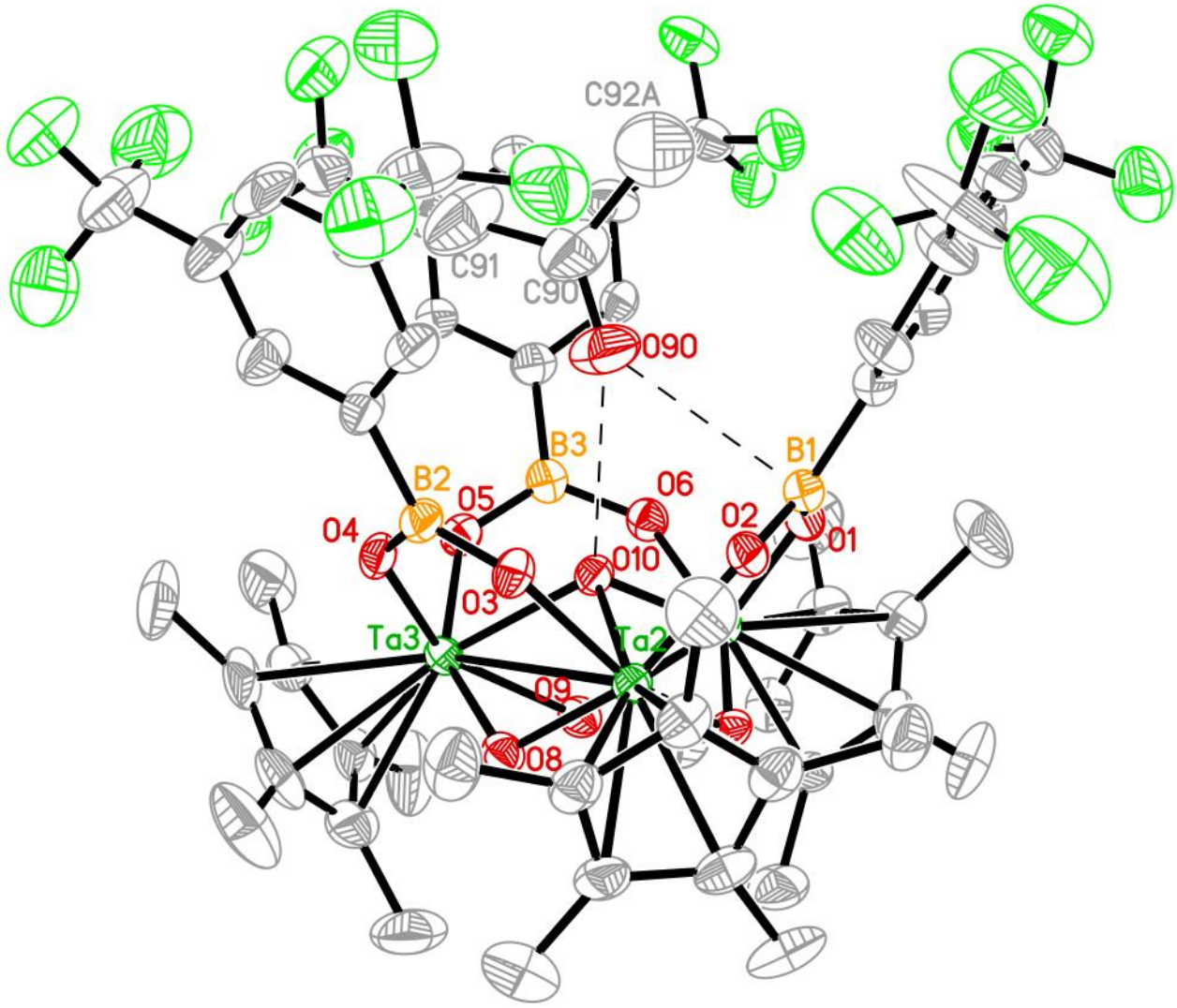

Figure 4.

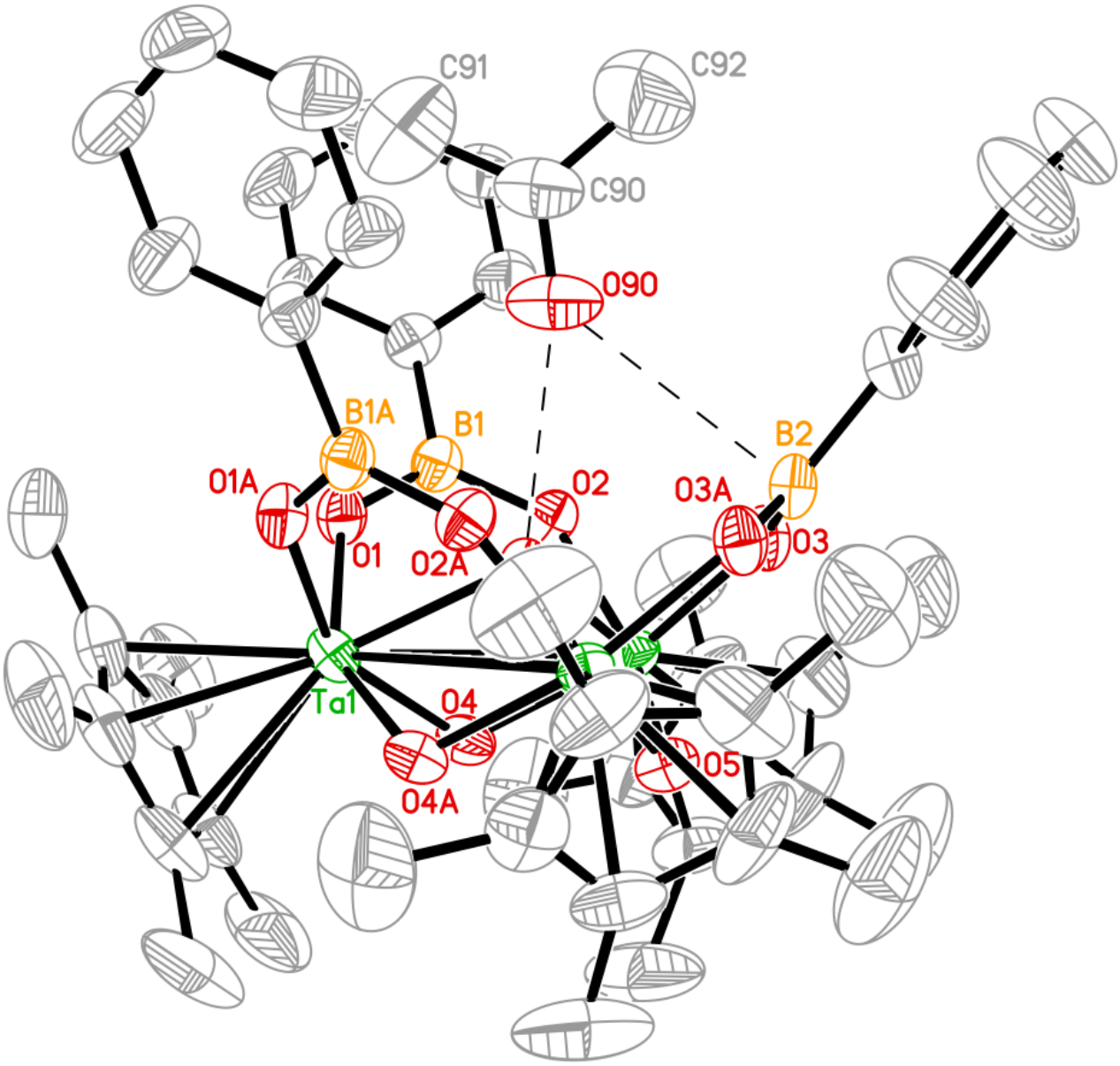

Figure 5.

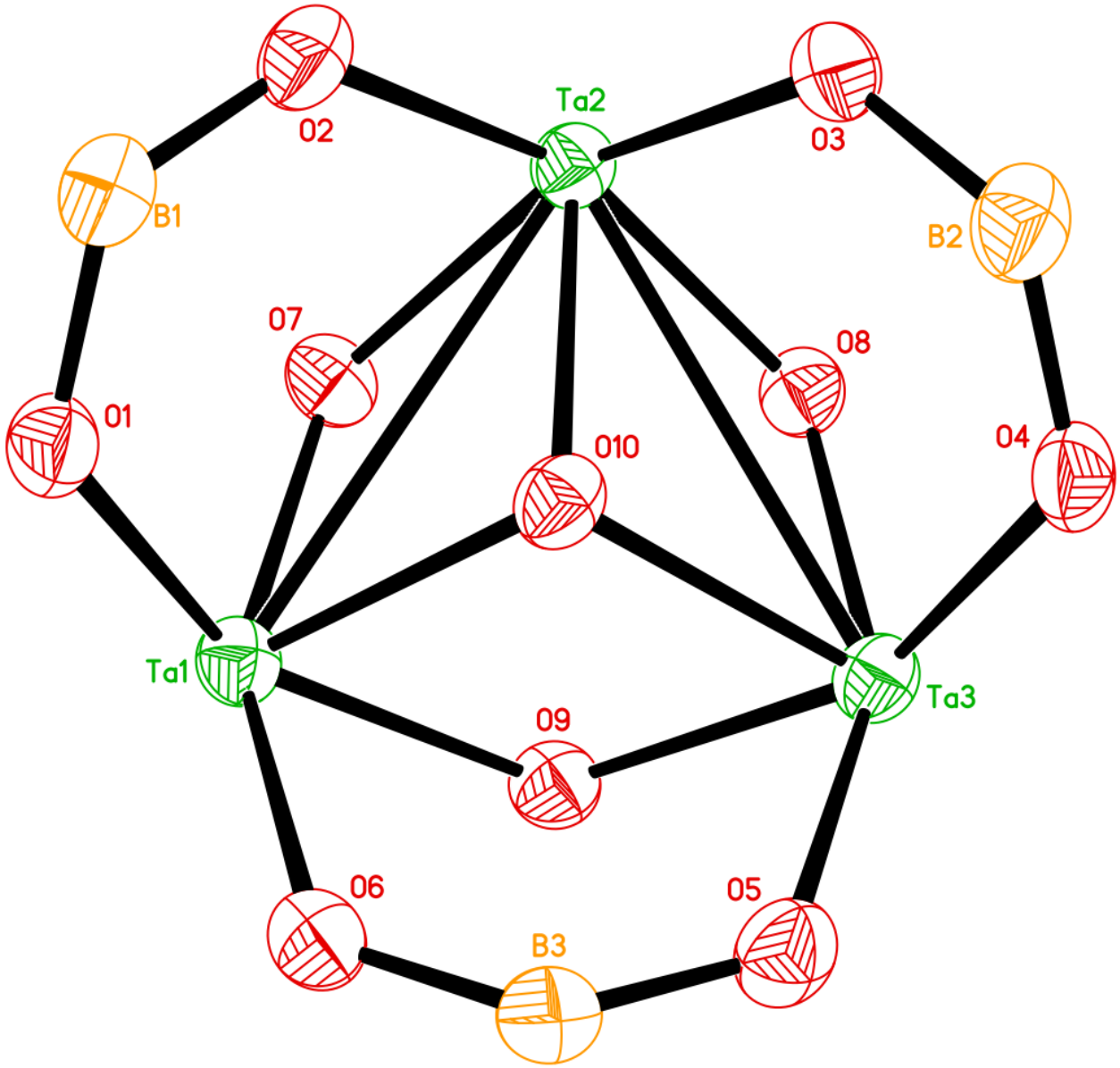

Figure 6.

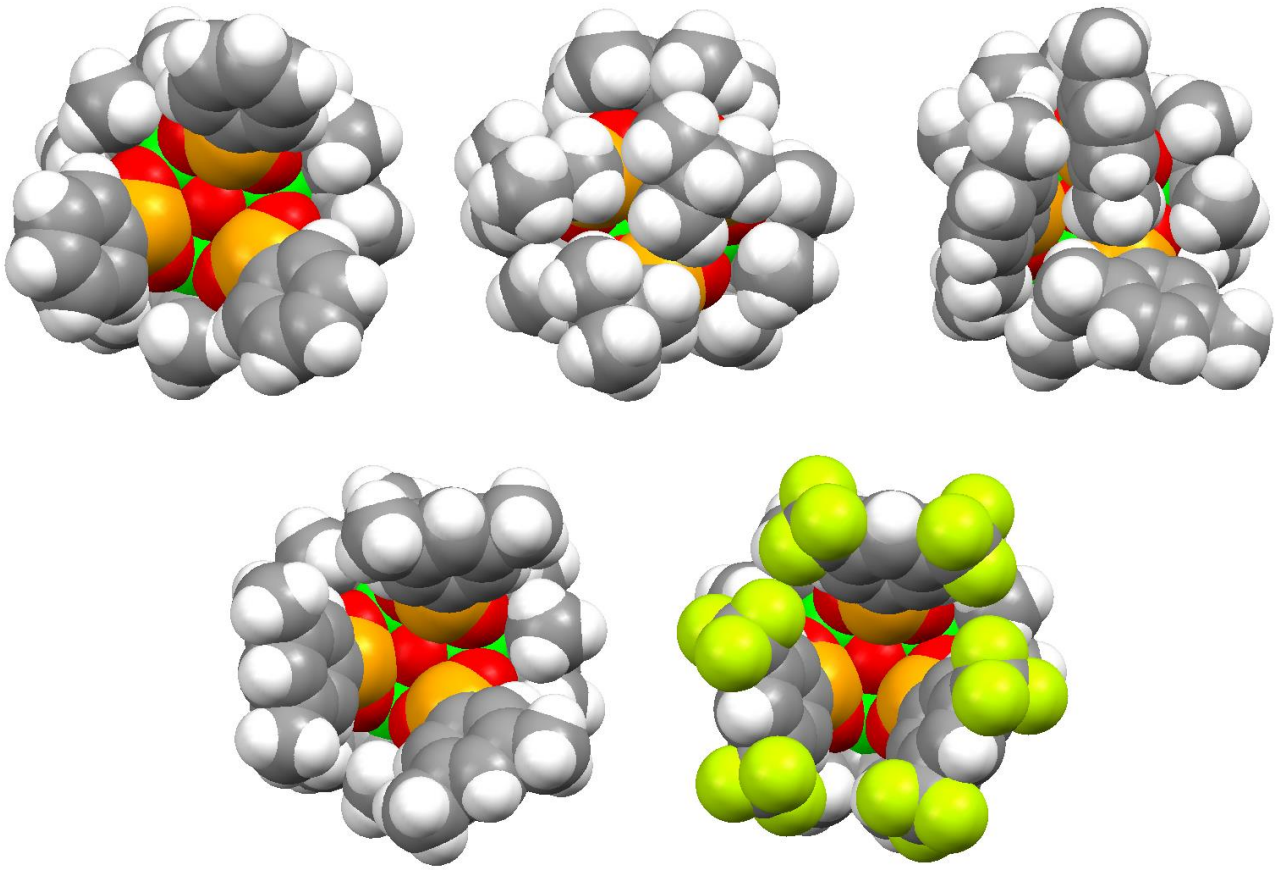

Figure 7.

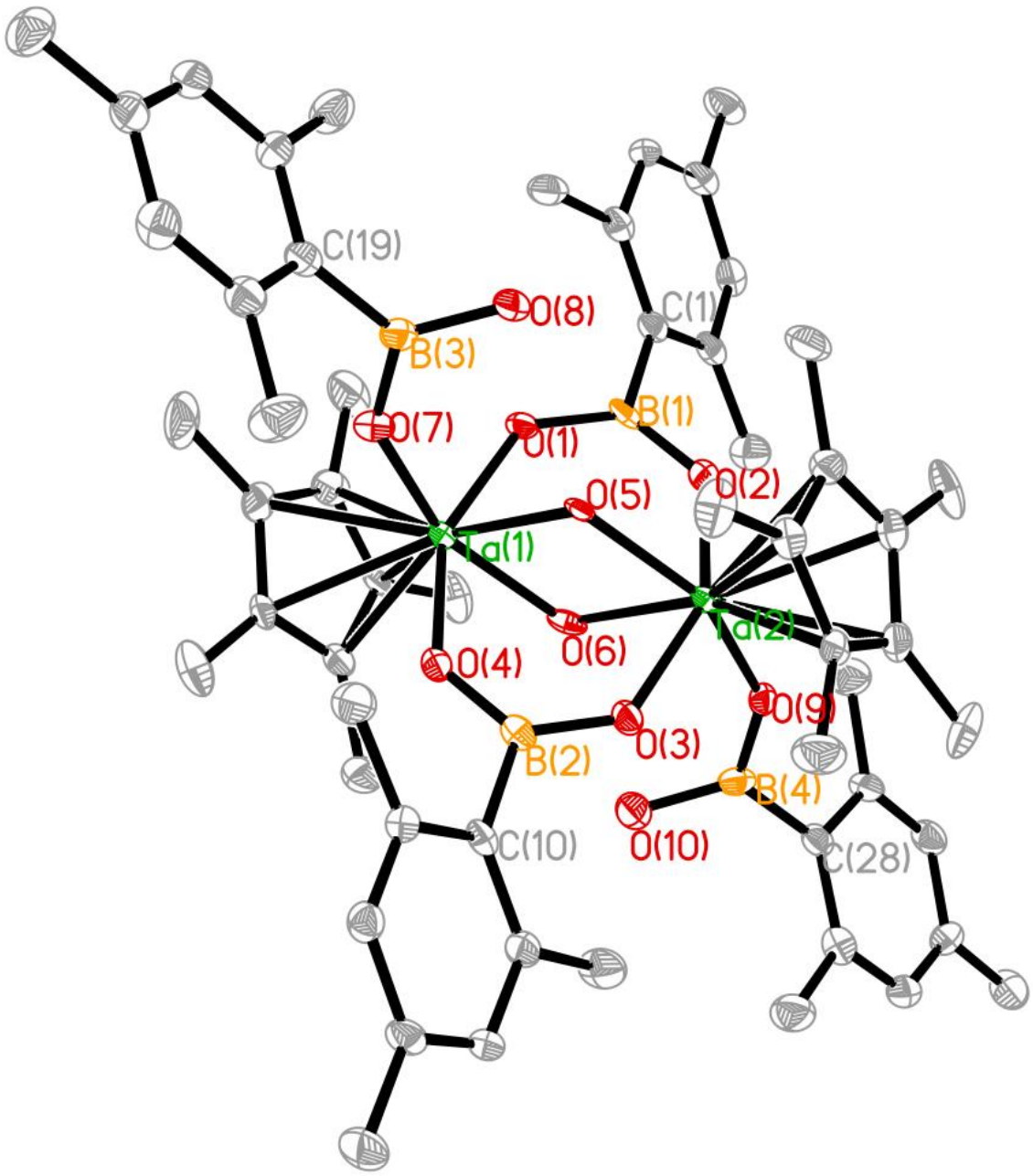

Figure 8.

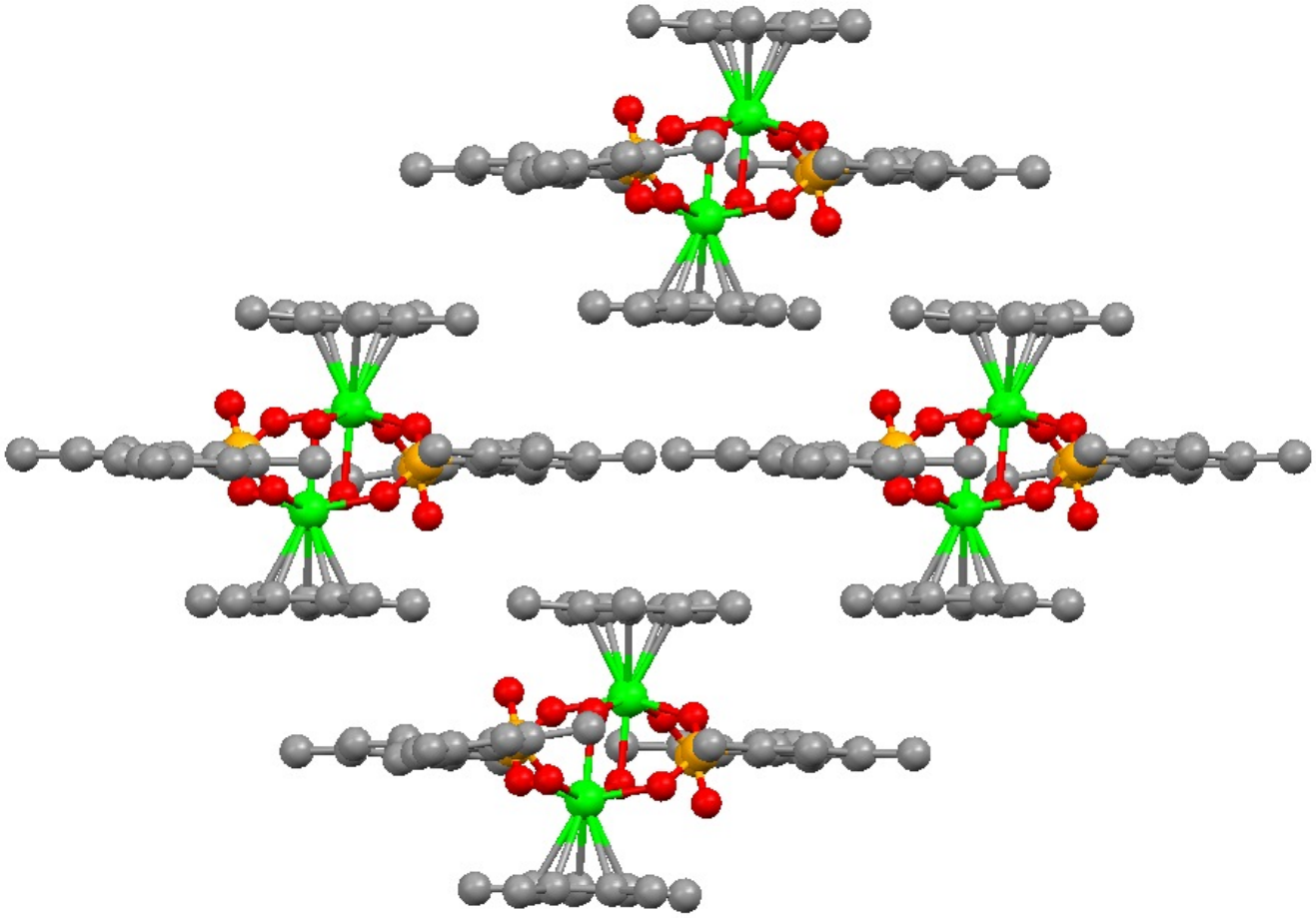

Figure 9.

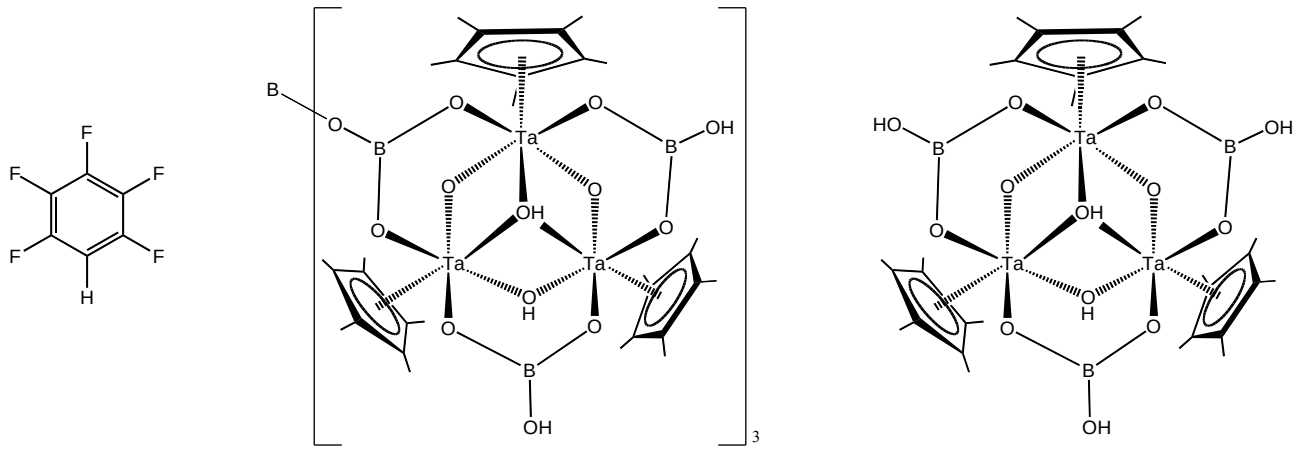
F
F
F
F
F
H
B
O
B
O
O
Ta
O
O
B
OH
O
O
OH
O
Ta
Ta
O
H
O
O
B
OH
3
HO
B
O
O
Ta
O
O
B
OH
O
O
OH
O
Ta
Ta
O
H
O
O
B
OH

Figure 10.

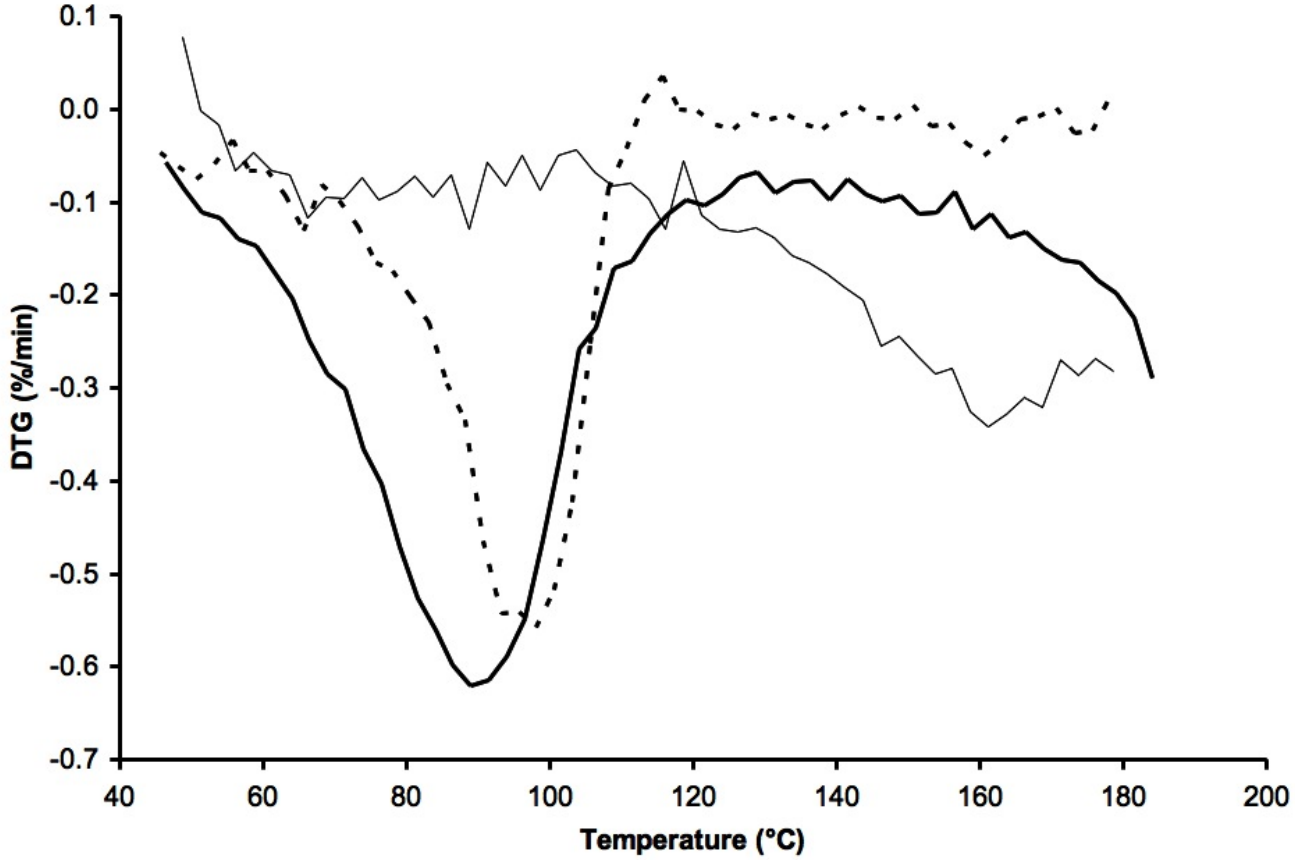
0.1
0.0
-0.1
-0.2
-0.3
-0.4
-0.5
-0.6
-0.7
DTG (%/min)
40
60
80
100
120
140
160
180
200
Temperature (°C)

Figure 11.

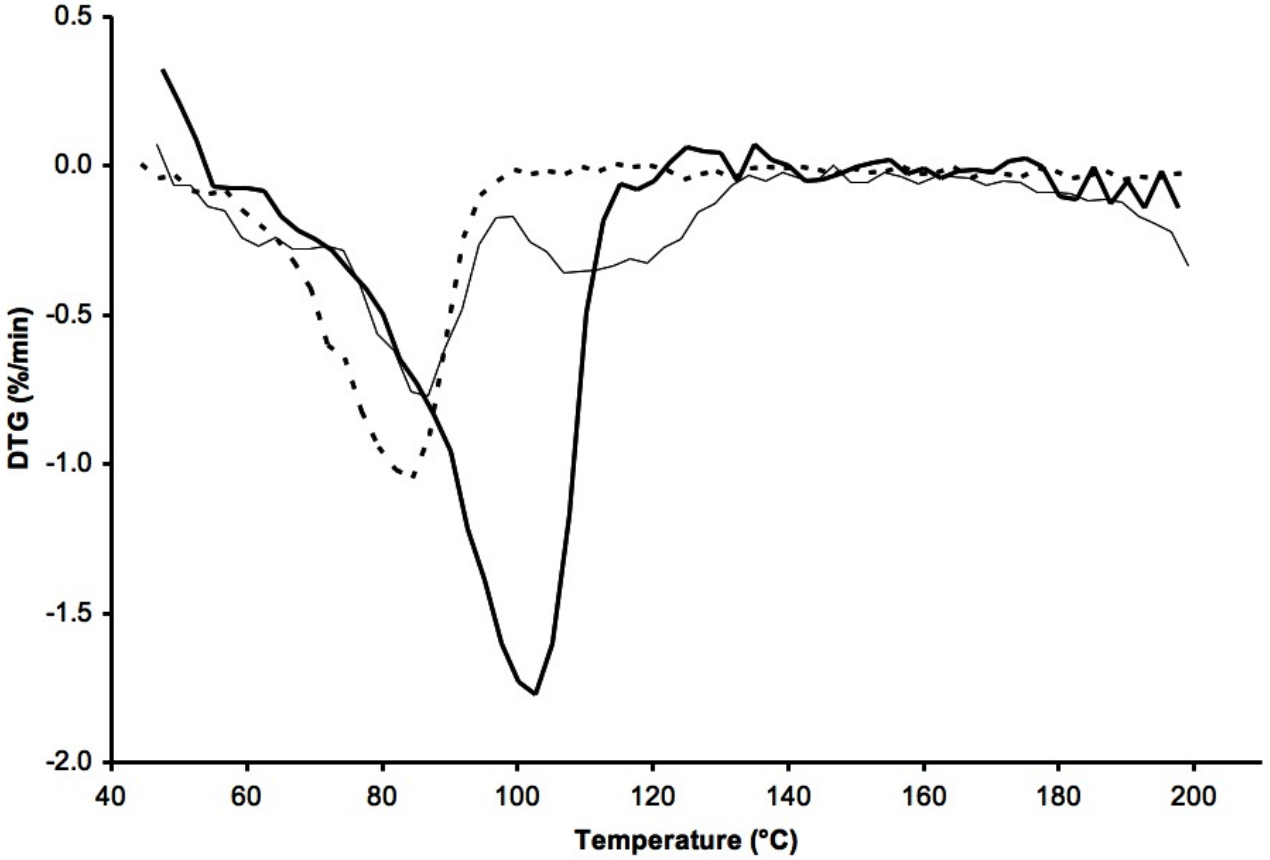
0.5
0.0
-0.5
-1.0
-1.5
-2.0
DTG (%/min)
40
60
80
100
120
140
160
180
200
Temperature (°C)

Figure 12.

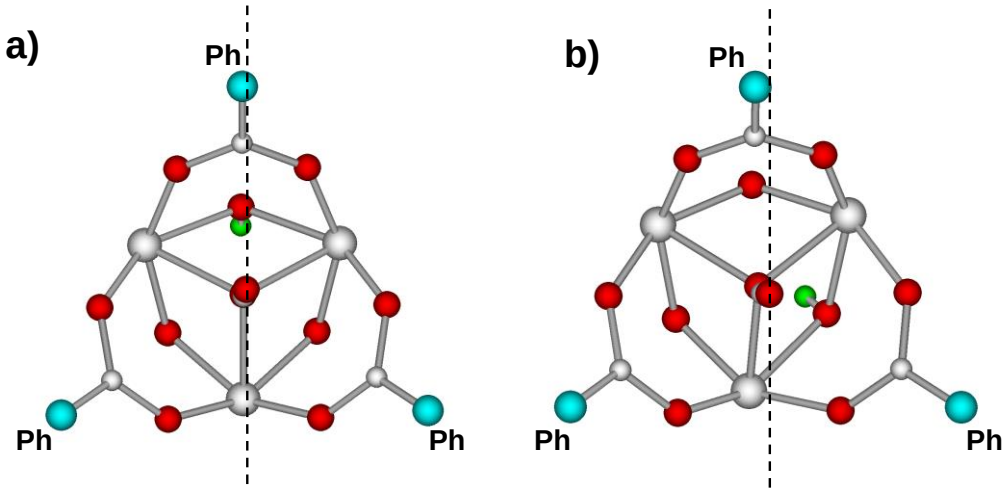

Figure 13.